Master's thesis

NTNU
Norwegian University of Science and Technology
Faculty of Natural Sciences
Department of Chemistry

Vilde Emilie Aas

Statistical Analysis of Paint Ingredients' Effect on Hydrophobicity and Surface Roughness

Using the Power Spectral Density Function to Quantify Roughness

Master's thesis in Chemical Engineering and Biotechnology
Supervisor: Angelika Brink and Solon Oikonomopoulos
June 2022

NTNU
Kunnskap for en bedre verden

Vilde Emilie Aas

Statistical Analysis of Paint Ingredients' Effect on Hydrophobicity and Surface Roughness

Using the Power Spectral Density Function to Quantify Roughness

Master's thesis in Chemical Engineering and Biotechnology
Supervisor: Angelika Brink and Solon Oikonomopoulos
June 2022

Norwegian University of Science and Technology
Faculty of Natural Sciences
Department of Chemistry

NTNU
Norwegian University of
Science and Technology

Abstract

As temperatures are rising globally due to greenhouse gas emissions and fuel prices continue to increase, the shipping industry is searching for solutions to decrease fuel expenditure. One solution proposed is the air-lubrication system, pumping air underneath the hull and creating a layer of air/water mixture decreasing the skin friction drag of the ship as it moves through water. This reduction in skin friction drag results in a significant decrease in fuel consumption. In order to optimise this effect, a coating solution which attracts air and repels water is proposed. Surfaces with this characteristic are called hydrophobic or superhydrophobic for highly water repellent surfaces. Extensive literature exists on how to design superhydrophobic surfaces on small scales, but not on an industrial scale. Therefore, the goal of this thesis is to explore the effect of different paint ingredients on hydrophobicity and surface roughness which is essential to create superhydrophobic surfaces.

Regression analyses were performed using paint ingredients as predictors and measured water contact angles (WCA) and roughness values as responses. Topography measurements were performed in order to calculate roughness values root mean square (RMS) roughness, slope and curvature using the power spectral density function (PSD). An examination of the different roughness values' effect on the WCA was conducted. Due to a lack of correlation, RMS roughness was not used further in the analysis, most likely as the RMS roughness was dominated by too large wavelengths. The RMS slope correlated too much with RMS curvature while displaying higher degrees of variance. RMS curvature was therefore chosen as the roughness value to represent surface roughness and used for further correlation.

The paint ingredients which showed the most promising results in the regression analysis were the Silikopon EF binder, a superhydrophobic additive and superhydrophobic functionalised diatomaceous earth (FDE) at high weight percentages. Further examination of results by fitted line plots showed that for high weight percentages of functionalised diatomaceous earth (FDE), the dependency on binder and additive in order to increase WCA's diminished. The most important factor to achieve high levels of WCA's was therefore high weight percentages of FDE, and the binder or the presence of the superhydrophobic binder was less important.

A wetting theory was proposed as fitted line plots highlighted some unexpected behaviour concerning high WCA's at low RMS curvature values which were not in alignment with state of the art theory. The wetting theory described three different levels of wetting: non-wetting, wetting by a thin layer of binder and wetting by a thick layer of binder. The level of wetting was assumed to affect how the particles define the roughness of the surface and the effect of the particles' hydrophobicity. Further work could include combining a hydrophilic binder with a hydrophobic particle or vice versa in order to encourage non-wetting and exposed hydrophobic or superhydrophobic particles at the surface. Microscopy methods with higher resolutions are needed in order to differentiate between microroughness and nanoroughness and to further investigate the proposed wetting theory.

Sammendrag

Siden globale temperaturer øker grunnet drivhusgassutslipp og drivstoffpriser fortsetter å heves, er skipsindustrien på jakt etter en måte å minske drivstofforbruket. En forslått løsning er luftsmøringssystemer som pumper ut luft under skroget på skip og lager en luft- og vannblanding for å minske friksjonsmotstanden til skipet når den beveger seg i vann. Denne reduksjonen i friksjonsmotstand vil redusere drivstofforbruket betydelig. For å optimalisere denne effekten trengs det et belegg på skroget som tiltrekker seg luft og avstøter vann. Overflater med en slik karakteristikk kalles hydrofobiske eller superhydrofobiske hvis overflaten har en høy grad av vannavstøting. Omfattende litteratur finnes om hvordan man kan designe superhydrofobiske overflater i en liten skala, men ikke på en industriell skala. Derfor er målet med denne avhandlingen å utforske effekten av ulike malingsingredienser på hydrofobisiteten og overflateruheten som er essensiell for å lage superhydrofobiske overflater.

Regresjonsanalyser var utført ved å bruke malingsingredienser som prediktorer og målte vannkontaktvinkler og ruhetsverdier som responsvariabel. Topografiske målinger av prøver ble utført for å regne ut ruhetsvariablene root mean square (RMS) roughness, slope og curvature ved bruk av power spectral density function (PSD). En undersøkelse av de forskjellige ruhetsverdienes effekt på vannkontakvinkelen var utført. På grunn av en mangel på korrelasjon ble RMS roughness ikke brukt videre i analysen, mest sannsynlig fordi den var dominert av for store bølgelengder. RMS slope korrelerte for mye med RMS curvature samtidig som den viste mer varians. På grunn av dette ble RMS curvature brukt som ruhetsverdien som skulle representere overflateruheten og ble brukt for videre korrelasjoner.

Malingsingrediensene som viste mest potensiale i regresjonsanalysen var Silikopon EF bindemiddelet, et superhydrofobisk additiv og superhydrofobisk funksjonalisert diatoméjord (FDE) ved høye vektprosenter. Videre undersøkelse ved bruk av spredningsplott med rette linjer som passet punktene viste at for prøver med høy vektprosent av FDE minket avhengigheten av bindemiddel og additiv for å få høye vannkontaktvinkler. Den viktigste faktoren for å øke hydrofobisiteten var altså en høy vektprosent av FDE og bindemiddel eller om det superhydrofobiske additivet var tilsatt var mindre viktig.

En teori om fukting ble foreslått da spredningsplottene fremhevet uventet oppførsel angående høye vannkontakvinkler med lave RMS curvature-verdier, som ikke følger litteraturen. Teorien om fukting beskriver tre ulike grader av fukting: ikke-fukting, fukting av et tynt lag bindemiddel og fukting av et tykt lag bindemiddel. Graden av fukting ble antatt å påvirke hvordan partiklene definerer ruheten til overflaten og effekten av partikkelens hydrofobisitet. Videre arbeider kan inkludere en kombinasjon av et hydrofobisk bindemiddel og hydrofile partikler og omvendt for å oppfordre til ikke-fukting og eksponerte hydrofobiske eller superhydrofobiske partikler på overflaten. Mikroskopiske metoder med høyere oppløsning trengs for å differensiere mellom mikroruhet og nanoruhet og for å utforske videre den foreslåtte teorien om fukting.

Preface

This thesis was written at the Department of Chemistry at the Norwegian University of Science and Technology in the Spring of 2022 in collaboration with Jotun AS and the Department of Mechanical and Industrial Engineering. It concludes my master's degree in Chemical Engineering and Biotechnology with a specialisation in Applied Theoretical Chemistry.

I would like to use this opportunity to show gratitude to everyone who has helped me along the way. First and foremost, I would like to thank my supervisor Angelika Brink who has provided guidance, great discussions and feedback throughout the semester. Your interest in my work was a constant motivation. I would also like to thank Kristin Søiland and Jamie Foster for helpful suggestions and sample preparations. Finally, I would like to thank Solon Oikonomopoulos for all the administrative work when collaborating with an external company for my thesis.

Table of Contents

List of Figures

List of Tables

1 Introduction

One of the largest threats to our planet today is climate change caused by the emissions of greenhouse gases (GHG). These emissions increase the global temperature which will result in consequences such as droughts, water scarcity, flooding, catastrophic storms and loss of biodiversity[1]. Therefore a reduction in GHG emissions is necessary in every economic sector. The shipping industry is responsible for 3% of the global GHG emissions and could increase by 250% within 2050 due to the growing demand for global trading[2, 3]. GHG emissions in the shipping industry has to be reduced. Unregulated, it could be responsible for 17% of the global emissions by 2050[3].

A potential new technology to decrease GHG emissions in the shipping industry is air lubrication systems. Depending on the type of vessel, up to 80% of a ship's energy consumption can be due to skin friction drag[4]. Air lubrication systems is situated in the hull of the ship and release air which coats the outer bottom of the hull with an air/water mixture[5]. This layer of air will decrease friction as the ship moves through the water. This decrease in friction will result in a significant decrease in fuel expenditure. This is highly favourable as it will both lower GHG emissions and combat high fuel prices. In order to fully utilise the effect of the air lubrication system an optimised coating solution is essential.

A coating solution supporting air-lubrication would ideally help the hull trap the air and repel water, reducing the amount of air needed to be pumped by the air lubrication system. Surfaces which repel water are called hydrophobic, or superhydrophobic with a higher degree of repulsion. It can be assumed that this characteristic is ideal when creating an optimised coating solution for air lubrication systems. In order to create a superhydrophobic surface, the chemical composition has to be hydrophobic and a degree of surface roughness needs to be present. Those surfaces have been explored rigorously in literature. However, often the solutions presented contain the highly electronegative fluorine and/or creating surface roughness by methods such as laser or moulding[6, 7, 8]. Fluorine is damaging to the environment and should be avoided, and using laser and moulding to achieve the ideal surface roughness is not viable on a large industrial scale. Therefore, this study will try to explore how to create a superhydrophobic coating without fluorine that possesses chemical hydrophobicity and a high level of roughness by randomly distributing the particles in the paint.

Regression analysis will be used to explore the effects of different paint ingredients on hydrophobicity and surface roughness. In order to quantify the surface roughness, the power spectral density function (PSD) of topography measurements will be used. The PSD, if used correctly, is independent of the measurement methods and resolutions, and it can be used to extract roughness parameters such as the root mean square roughness. The results of the regression analysis will be used to discuss the most promising paint ingredients and composition for an optimised coating solution for air lubrication systems. Finally, in order to explain some unexpected behaviour concerning water contact angles and roughness values, a wetting theory is proposed.

2 Theory on surfaces

2.1 Surfaces and surface free energy

An interface is the physical boundary between two phases. There are mainly three types of interfaces: solid-liquid, solid-vapour and liquid-vapour. A solid or liquid interfaced with a vacuum is called a surface, though usually the solid-vapour and liquid-vapour interfaces are also referred to as surfaces.[9]

At the phase boundaries, the molecules of the two phases will act differently compared to the bulk molecules. The bulk molecules will interact equally with each other, creating a net force of zero. Whereas, at the phase boundary there is a difference in interactions which results in an excess surface free energy. The surface free energy is equivalent to the work done to create a surface of unit area (Jm^{-2}). Systems will try to minimise surface free energy, which is why liquid droplets contracts spontaneously.[9]

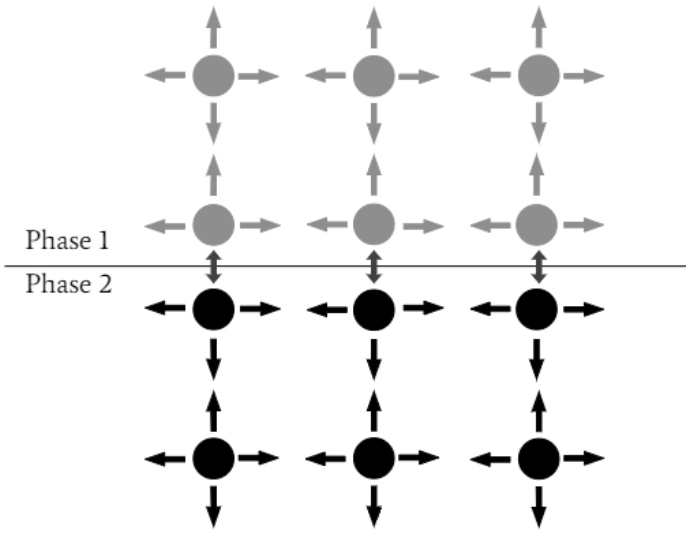

Figure 1: Schematic representation of the difference in interactions between molecules at the surface and the bulk molecules

For liquids the term surface tension is highly relevant. As liquid molecules are subjected to cohesion forces they are kept close to each other. The surface molecules are not exposed to liquid molecules from all sides and consequently feel a net force towards the bulk molecules. Therefore, the system will act as a simple pulley, as illustrated in Figure 2, where surface tension occurs due to surface molecules being attracted to each other while feeling a downward pull towards the bulk. The surface tension causes the liquid to behave as though surrounded by an invisible membrane. Surface tension has units force per length.[10]

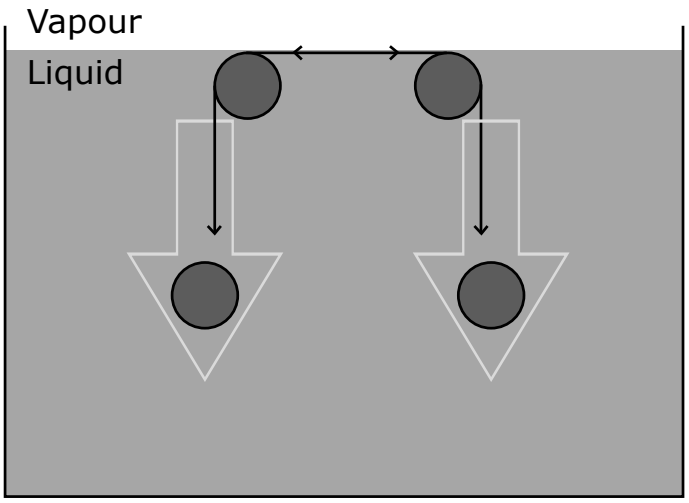

Figure 2: Schematic illustration of the interaction of liquid molecules at the surface resulting in an interfacial tension. The molecules act like simple pulleys as the surface molecules interact with each other while exhibiting a force downwards from the bulk molecules. Amended from [10].

2.2 Contact angle

The contact angle (CA), θ, is the angle where a liquid-vapour interface meets a solid and serves as a quantitative evaluation of the wetting of a solid by a liquid[11]. It can be measured by releasing a liquid droplet onto a surface and measuring the angle at the three-phase boundary where the liquid, solid and vapour phases meet, as depicted in Figure 3. It is used to evaluate the surface free energies as the liquid drop will change its shape depending on the liquid-solid and liquid-vapour interactions. The most common probing fluid is water, and the measured contact angle is called the "water contact angle" (WCA).[12]

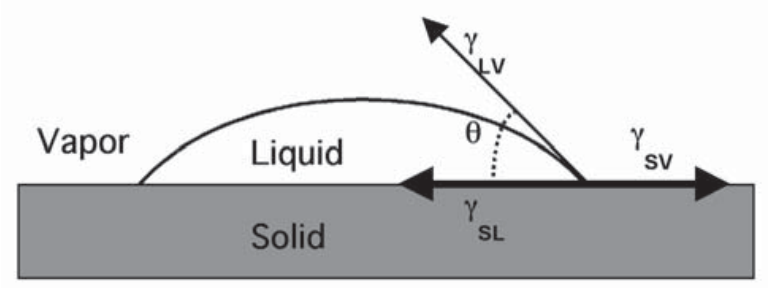

Figure 3: Schematic drawing of a liquid droplet on a surface in a surrounding vapour forming the contact angle, θ[13].

The contact angle will vary according to the liquid's surface tension and the surface free energy of the solid, illustrated in Figure 4. For low surface energy solids and high liquid tension, there will be non-wetting, resulting in a large observed CA. On the other hand, for high surface free energy solids and low liquid surface tension, wetting will occur and the liquid drop will spread, resulting in a low CA. When observing a WCA in air, only the solid surface and its surface free energy can affect the WCA as the liquid surface tension is set.[14]

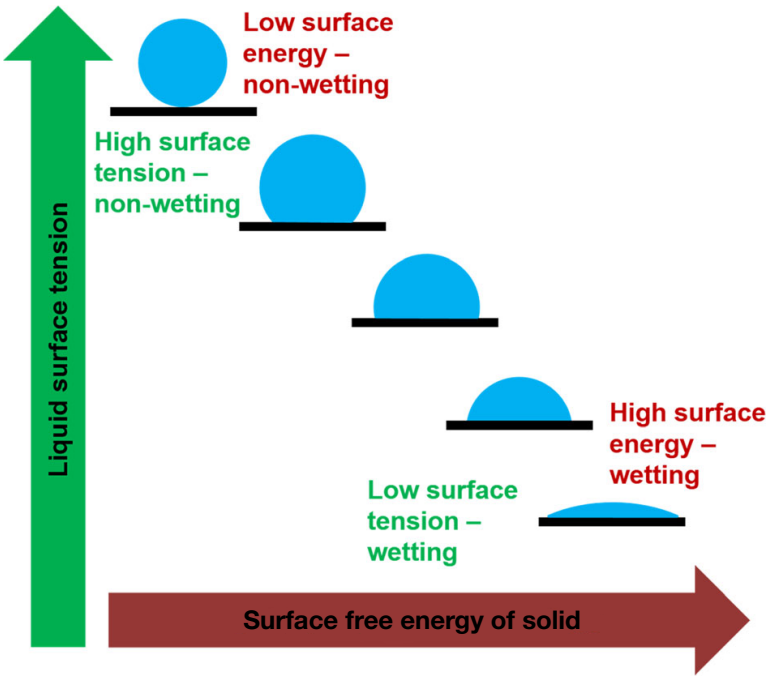

Figure 4: Schematic drawing of the relation between the level of wetting, the liquid surface tension and the surface free energy of the solid. High liquid surface tension and low surface free energy of solid results in non-wetting. Wetting occurs when the liquid surface tension is low and the surface free energy of the solid is high.[14]

Typically, one separates the level of wetting into two categories: non-wetting and wetting. Non-wetting occurs when the observed CA is larger than 90°, and a solid surface which displays a WCA larger than 90° is referred to as being hydrophobic. On the other hand, wetting occurs when the CA is less than 90° and solids displaying WCA's less than 90° is referred to as being hydrophilic.

Young proposed a relationship between the contact angle and the three interfacial forces involved,

$$\gamma_{SV} = \gamma_{SL} + \gamma_{LV} \cos\theta, \tag{1}$$

where γ_{SV}, γ_{SL} and γ_{LV} are, respectively, the solid-vapour, solid-liquid and liquid-vapour interfacial force per unit length of the contact line[15]. The relation is represented with vectors in Figure 3. Young's equation is a balancing of forces, but it can also be derived by minimising the system's surface free energy[16].

2.3 Surface roughness

The above section relates contact angles to the inherent chemistry of the phases involved, such as the surface free energy of the solid and liquid-vapour interfacial tension. In this paper, how the chemistry of the phases affect the level of hydrophobicity of the surface will be referred to as "chemical hydrophobicity". In addition to the inherent chemistry of the phases, the physical nature of the solid, mostly its degree of roughness, will also affect the level of wetting. Mainly two theoretical models have been developed to explain the surface roughness' effect on the contact angle, namely the Wenzel model and the Cassie-Baxter model.

Wenzel introduced a roughness factor, r, to Young's equation which is defined as

$$r = \frac{A}{A_0}, \tag{2}$$

where A is the actual area of a rough surface and A_0 is the area of an ideal, smooth surface[17]. Young's equation is then modified to[18]

$$r(\gamma_{SV} - \gamma_{SL}) = \gamma_{LV} \cos\theta_{\text{rough}}. \tag{3}$$

The contact angle θ_{rough} refers to a droplet's contact angle on a rough surface as opposed to θ_{smooth} which will be used to refer to the contact angle of an ideal smooth surface.

The Wenzel model is based on the assumption that the liquid will wet all the grooves of the solid surface on which it is placed on. Thus, the total interaction between the liquid and the solid will be higher than for a smooth surface, resulting in a magnification of the wetting properties exhibited by the smooth surface. This will affect the contact angle in the two following ways:[17]

$$\theta_{\text{smooth}} < 90^\circ \rightarrow \theta_{\text{rough}} < \theta_{\text{smooth}} \tag{4}$$

$$\theta_{\text{smooth}} > 90^\circ \rightarrow \theta_{\text{rough}} > \theta_{\text{smooth}} \tag{5}$$

According to Wenzel, if the contact angle, θ, is less than 90° then the rough surface will enhance this property and reduce θ. If, on the other hand, θ is larger than 90° then this will further increase θ. This effect is depicted in Figure 5.[17]

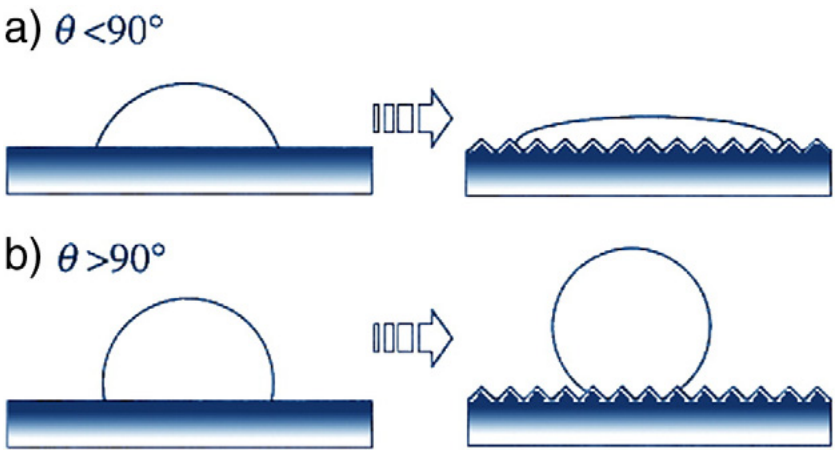

Figure 5: Schematic drawing of the enhanced wetting properties due to roughness according to the Wenzel model[19].

Following the Wenzel model, one can show that the relationship between the CA of a rough and smooth surface is proportional and the roughness factor is the constant of proportionality,

$$\cos\theta_{\text{rough}} = r \cos\theta_{\text{smooth}}. \tag{6}$$

This relationship is graphically displayed in Figure 6. The range of roughness factors in Figure 6 does not represent real roughness factors, which could be thousands, even millions, of times larger depending on the resolution of the surface measurements.

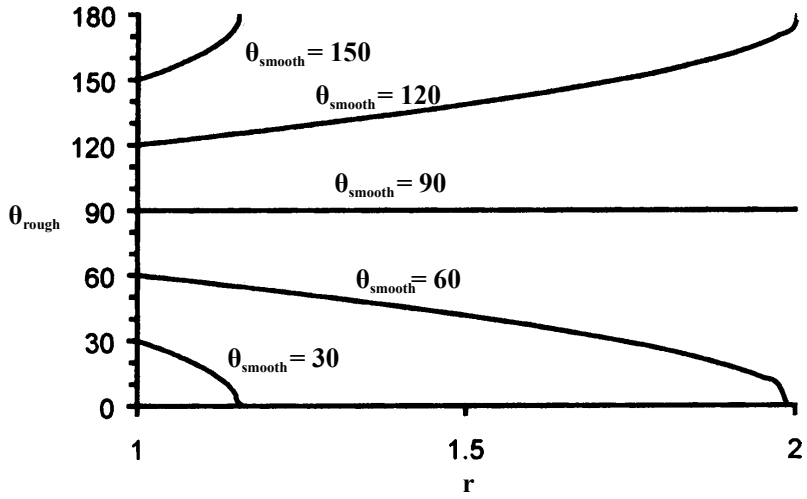

Figure 6: Graphs showing the CA of a rough surface, θ_{rough}, as a function of the roughness factor, r, for different values of the CA of a smooth surface, θ_{smooth}, according to the wetting model proposed by Wenzel. Amended from [20].

The Cassie-Baxter state describes a composite surface where the liquid droplet is situated on top of the asperities and does not wet the grooves of the surface[21]. It, therefore, describes a partially wetted rough surface as opposed to the Wenzel model which describes a fully wetted rough surface. The visual difference between the three wetting models is illustrated in Figure 7. Young's equation is again modified, now to include a representation of a composite surface,

$$\cos\theta_{\text{rough}} = r f_1 \cos\theta_{\text{smooth}} - f_2 \tag{7}$$

where f_1 and f_2 are the area fractions for the wetted and non-wetted surface respectively. The non-wetted surface in this case is the grooves underneath the droplet which are filled with vapour[21]. Unless the roughness factor is relatively large, θ_{rough} will be larger than θ_{smooth}[22].

The difference between the two models can be observed by measuring the roll-off angle of the surface. The roll-off angle is the angle at which the surface has to be tilted for a liquid droplet to roll off the surface. It serves as a measure of adhesion of the liquid droplet to the surface. The Wenzel state is "sticky" due to the liquid droplet fully wetting the surface and therefore has a high roll-off angle and high adhesion. The Cassie-Baxter state is "slippery" and has a low roll-of angle and low adhesion due to the surface only being partially wetted.[23]

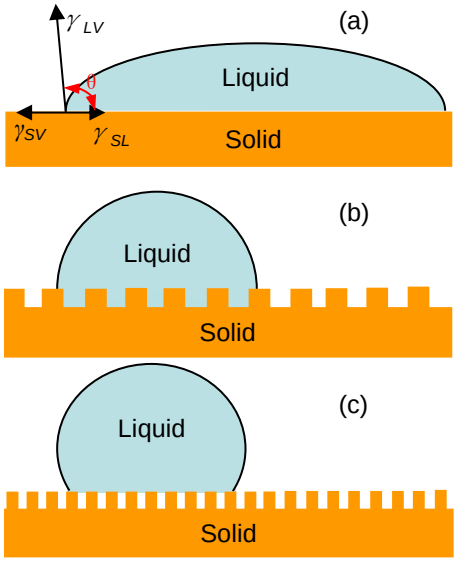

Figure 7: Schematic drawing of the three wetting models Young (a), Wenzel (b) and Cassie-Baxter (c)[12].

2.3.1 Fractal surfaces

Surfaces inhibit roughness on all scales and will often be of a self-affine fractal nature, meaning they will look similar when magnified and scaled accordingly in the horizontal, lateral and vertical directions[24]. Figure 8 shows a surface depicting fractal behaviour. Self-affine fractal surfaces may exhibit roughness all the way from their lateral size and down to the atomic scale[24].

When magnifying a fractal surface, the scaling behaviour will follow the Hurst exponent, H. If scaling the horizontal and lateral direction by r, the surface will remain statistically the same if the vertical direction is scaled by r^H[25]. The Hurst exponent is between 0 and 1 and is related to a non-integer fractal dimension, D_f. The fractal dimension is $D_f = 3$ - H for surfaces and $D_f = 2$ - H for a cross-sectional profile[25]. For surfaces, this means that the fractal dimension is larger than 2 and typically between 2.1 and 2.3[26]. Fractals of higher dimensions are rare as they will have a very high level of roughness which will make them fragile and sensitive to external objects smoothing the surface[27].

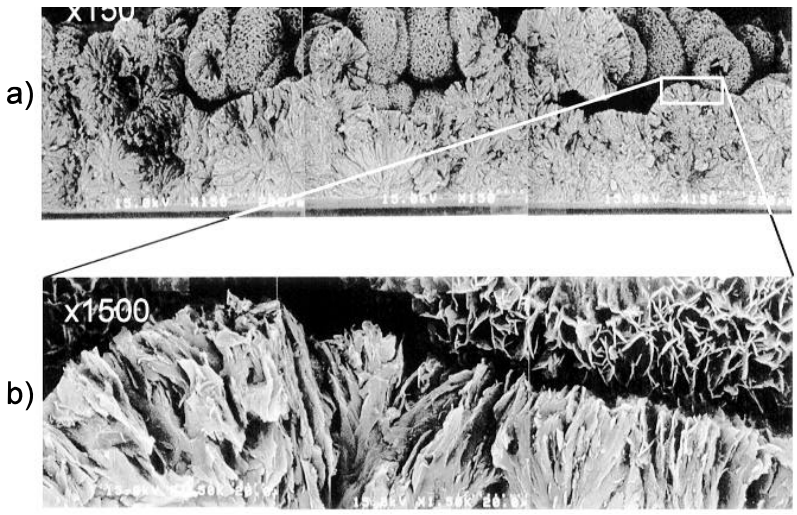

Figure 8: SEM images of a cross-section of a surface displaying fractal behaviours where the magnifications are x150 (a) and x1500 (b)[28].

2.3.2 Superhydrophobicity

A superhydrophobic surface is defined as having a WCA of at least 150° and a contact angle hysteresis (CAH) of less than 10°. The CAH is the difference between the advancing CA and the receding CA. It can be measured by doing a roll-off experiment or using the sessile drop method by adding liquid to a droplet to measure the advancing CA and removing liquid to measure the receding CA. These methods are demonstrated in Figure 9. The high CA indicates that the surface repels water and low CAH signifies low adhesion of water to the surface and both are necessary to classify a surface as superhydrophobic.[29]

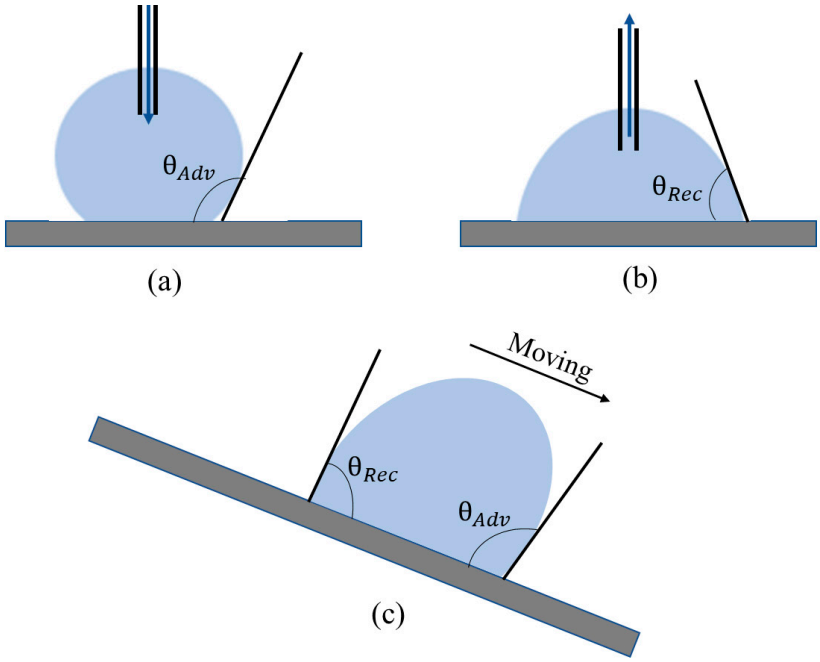

Figure 9: (a,b) Schematic drawing of the advancing and receding angle of the surface while performing the sessile droplet method, and (c) schematic drawing of advancing and receding angle during a roll-off experiment. [30]

The roughness of the surface is important for obtaining high WCA as the maximum WCA obtained for a smooth surface is around 120°[31]. The field of biomimetics, which involves mimicking nature for engineering applications, has played a large role in the understanding of roughness' effect on hydrophobicity. The lotus leaf has a WCA of around 160° and CAH of only a few degrees. In addition to being covered in a hydrophobic wax coating, it also possesses a naturally occurring roughness on two range scales: microroughness and nanoroughness[32]. Roughness at different scales is referred to as hierarchical roughness and serves as stability for the composite state, or the Carrie-Baxter state, where air is trapped in the grooves of the surface[33]. Figure 10 illustrates the different types of roughness.

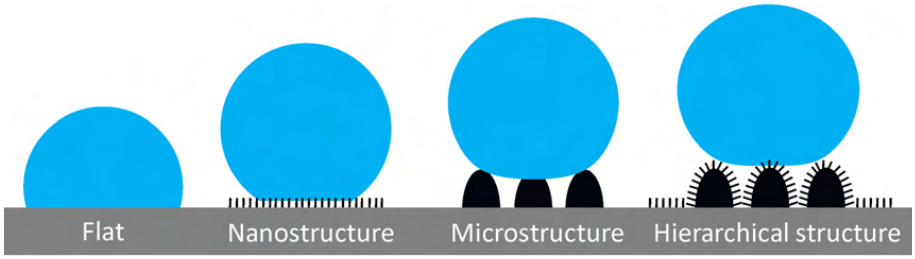

Figure 10: Schematic drawings of a flat, a nanostructured, a microstructured and a hierarchical structured surface[34].

Based on the functionality of the lotus leaf, Nosonovsky and Bhushan (2007) developed a set of criteria to achieve a stable superhydrophobic surface:

- The surface roughness should be hierarchical from micro- to nanoscale.
- The asperities should be high, but limited by the requirement to remain structurally strong.
- At each scale, the asperities should be narrow and far apart. This is however limited by factors such as the emergence of capillary waves which could fill the grooves with water and destabilise the composite state.
- The asperities at the nanoscale should be convex, meaning bumps and not grooves, in order to stabilise the composite state.
- The surface chemistry of the uppermost layer of the surface should be of a hydrophobic nature.

In order to create a superhydrophobic surface, several of these criteria are critical. For volumetric superhydrophobic coatings with a random roughness distribution the criteria hydrophobic chemical composition and hierarchical and convex roughness are relevant. A volumetric superhydrophobic coating is a coating which has superhydrophobic properties from its surface and all the way to the underlying substrate[35].

2.3.3 Quantifying surface roughness

Due to the fractal nature of surfaces, quantifying their roughness is challenging. Many roughness parameters have been developed and applied to overcome this challenge, but it is not possible to characterise the surface roughness with only one of these. The roughness

parameters are highly dependent on the magnification in which the surface is measured. Therefore a roughness value of a large section of the surface will vary greatly compared to the one calculated for a smaller section.

Two of the most widely used roughness parameters are the arithmetic roughness, R_a, and the root mean square (RMS) roughness, R_q. The arithmetic roughness is defined as the average deviation from the mean line over one sampling length and is usually averaged over consecutive sampling lengths[36]. The mathematical definition on a one-dimensional line scan in the x-direction is

$$R_a = \lim_{L\to\infty} \frac{1}{L} \int_{-L/2}^{L/2} |z(x) - \overline{z}| dx, \tag{8}$$

where L is the sampling length, z(x) is the height at position x and $\overline{z}$ is the average height across the sampling length. The RMS roughness is similar but is defined as the average root mean square deviations from the mean over the sampling length[36]. Its mathematical definition is

$$R_q = \sqrt{\lim_{L\to\infty} \frac{1}{L} \int_{-L/2}^{L/2} [z(x) - \overline{z}]^2 dx}. \tag{9}$$

One of the disadvantages of these two roughness parameters is that single, non-typical high peaks or grooves will be averaged out and affect the roughness values minimally. This means that the parameters will not give any information of the shape or irregularities of the surface. The main difference between representing the roughness by R_a versus R_q is that valleys and peaks will have a higher significance when using R_q due to the heights being squared.[37]

Other parameters one can use to describe the surface, following the RMS roughness, are the RMS slope (R'_q) and RMS curvature (R''_q). The RMS slope is the RMS of the first derivative of the surface profile[38]

$$R'_q = \sqrt{\lim_{L\to\infty} \frac{1}{L} \int_{-L/2}^{L/2} \left[\frac{dz}{dx} - \overline{z}'\right]^2 dx}, \tag{10}$$

where $\overline{z}'$ is defined as

$$\overline{z}' = \lim_{L\to\infty} \frac{1}{L} \int_{-L/2}^{L/2} \frac{dz}{dx} dx. \tag{11}$$

The RMS curvature is the RMS of the second derivative of the surface profile[38]

$$R''_q = \sqrt{\lim_{L\to\infty} \frac{1}{L} \int_{-L/2}^{L/2} \left[\frac{d^2z}{dx^2} - \overline{z}''\right]^2 dx}, \tag{12}$$

where $\overline{z}''$ is defined as

$$\overline{z}'' = \lim_{L\to\infty} \frac{1}{L} \int_{-L/2}^{L/2} \frac{d^2z}{dx^2} dx. \tag{13}$$

The RMS curvature is related to the sharpness of peaks and grooves on the surface. The hypothetical surfaces shown in Figure 11 and Figure 12 have the same R_q and a higher R'_q, and their level of perceived roughness differs greatly. The values for R''_q are especially contrasting, which highlights its importance when quantifying surface roughness. The surface in Figure 12 has an infinitely high R''_q due to the function being discontinuous, but

for a real surface this would be a finite number that could be used to distinguish between the two surfaces.[39]

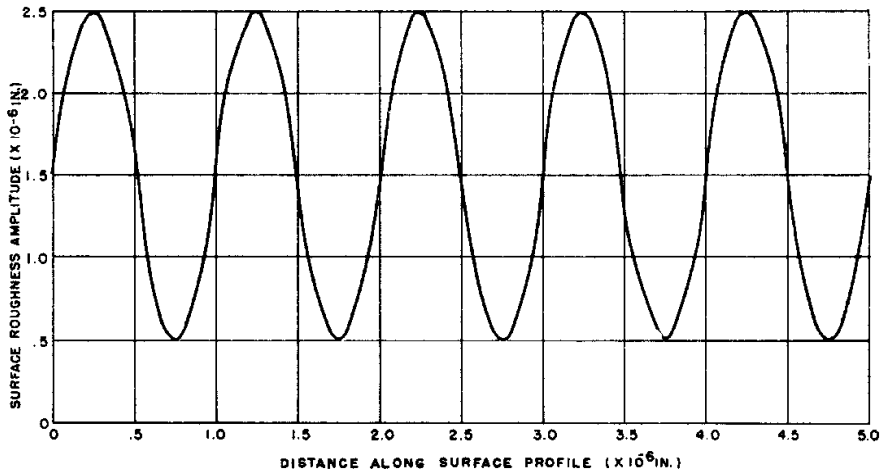

Figure 11: Hypothetical surface constructed from a sine wave with roughness values R_q = 17.9 nm, R'_q = 17.9 (dimensionless) and R''_q = 17.9 nm^{-1}[39].

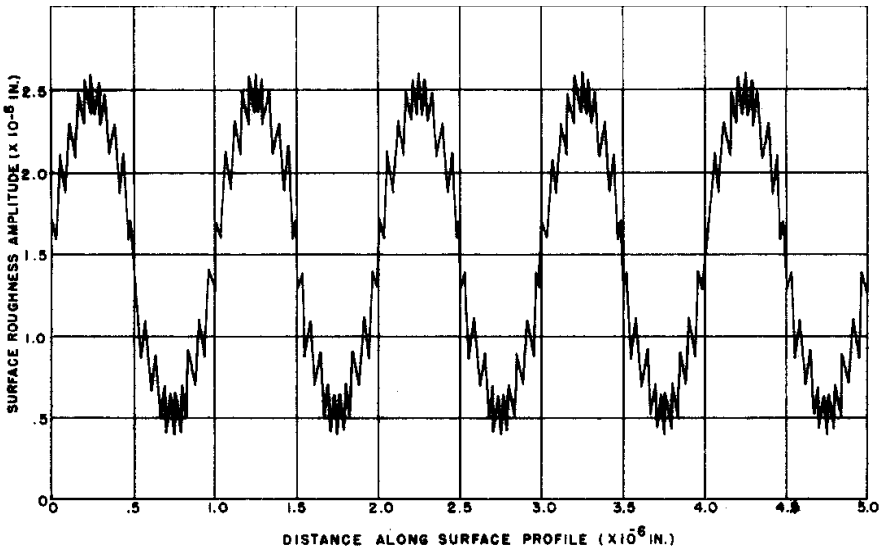

Figure 12: Hypothetical surface constructed from a sine wave and triangular wave with roughness values R_q = 17.9 nm, R'_q = 25.5 (dimensionless) and $R''_q = \infty$ nm^{-1}[39].

3 Methodology

3.1 Preparation of samples

In order to map the effect of paint ingredients on the WCA, and consequently the roughness and hydrophobicity, samples were prepared with different combinations and amounts of binders, additives and particles. All formulations were applied by draw down on PVC or glass plates.

Silikopon EF is a silicone-epoxy resin, and the Epoxy binder contain the organic compound bispehnol A diglycidyl ether (DGEBA). Some samples were made with Dowsil binder which is a reactive alkoxy-siloxane resin. The additive Tego Phobe 1505 (TP) was used to increase the hydrophobicity of the binder system.

Samples were made with lambda values 0, 0.2, 0.4, 0.6, 0.8, 1.0 and 1.2. The lambda value, Λ, describes the ratio between the amount of binder and amount of particles, and gives an indication of the amount of wetted particles by the binder in the formulation. It is defined by

$$\Lambda = \frac{PVC}{CPVC}. \tag{14}$$

PVC is the pigment volume concentration or the fractional volume of pigment in the dry coating[40]. At the critical pigment volume concentration, CPVC, there is just enough binder to wet all the particles in the coating. Increasing PVC above the CPVC, or $\Lambda > 1$, should result in a drastic change of the coating properties. In the context of roughness, increasing Λ will allow particles to be exposed at the surface and increase the surface roughness.

Functionalised diatomaceous earth (FDE), aerosil and nanosilica were particles used to attempt to increase the hydrophobicity and roughness of the surfaces. Diatomaceous earth is siliceous remains of diatoms[41]. It is chemically inert, porous, of low density and naturally varies in size which could contribute to a hierarchical roughness. The diatomaceous earth used was hydrophobically functionalised. Aerosil is a type of hydrophobic fumed silica and has a smaller particle size than FDE. The nanosilica used was hydrophobic and between 20 and 30 nm in size.

Seven water contact angle measurements were performed on each sample using a drop shape analyser. The average of these for each sample was used in the linear regression models.

3.2 Topography measurements

The measurements of surface topography were performed with the Sensofar metrology S Neox microscope using two optical techniques, confocal microscopy and interferometry. The level of magnifications used were 5x, 10x, 20x and 50x. Table 1 displays details of the measurement resolutions and sizes.

Table 1: Magnifications (Mag.), resolutions (Res.) and image size used for topography measurements of the surfaces.

Technique	**Mag.**	**Res. [μm per pixel]**	**Horizontal $\times$ lateral size [μm]**
Confocal	5x	1.38	3380 $\times$ 2830
Confocal	10x	0.69	1690 $\times$ 1410
Confocal	20x	0.35	845 $\times$ 707
Interferometry	50x	0.14	339 $\times$ 282

Measurements were performed by focusing on the samples and adjusting the brightness. The vertical range was set by moving the microscope until the sample was out of focus both above and below the focus point.

All measurements were processed using SensoMap software. A tilt compensation was performed to achieve an average slope of zero and missing points were restored.

3.3 Data analysis - the power spectral density function

The power spectral density function (PSD) can be calculated from the surface topography and used to quantify the surface roughness[42]. If used correctly, one can calculate roughness values while being mostly independent of the resolution and magnification of the measurements as the PSD contain statistical information about the surface[26]. The PSD is a form of signal analysis and is defined as the Fourier transform of the autocorrelation function of the signal. It detects the wavelengths in the signal, in this case the surface topography, and thus decomposes the surface into contributions from spatial frequencies[26]. Its physical meaning is the surface height squared per spatial frequency[43]. Spatial frequency is the inverse of the wavelength multiplied by 2π. The RMS roughness, slope and curvature can be extracted directly from the PSD and can be used to represent different scales of roughness. The RMS roughness is mainly determined by larger scale roughness, whereas the slope and curvature is increasingly dependent on the smaller scale roughness[26].

There are several ways in which to calculate the PSD of a surface. The most common method is the one-sided 1D PSD, which has cubic length units. It can be computed from a 1D signal, e.g. a line-scan, and is usually averaged over several measurements. A log-log plot of this plotted against the spatial frequency (q_x) with units per length is depicted in Figure 13. This method is denoted by $C(q)^{1D+}$ and is possible to calculate with most software packages that deals with PSD's. It is one-sided, denoted by the plus sign, as the PSD is symmetric around $q_x = 0$. Another PSD which is frequently used in literature is the one-sided isotropic PSD, $C(q)^{iso}$ which can only be used for isotropic surfaces, meaning the roughness of the surface is approximately the same in all directions. It is important to keep in mind that roughness parameters are extracted differently based on the specific PSD used.[26]

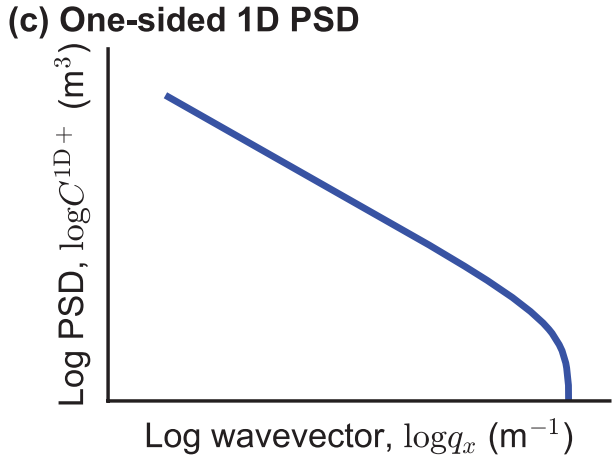

Figure 13: Ideal log-log plot of a PSD function[26].

The PSD typically consist of two regions, the "self-affine" region for high spatial frequencies (small wavelengths) and the "roll-off" region for low spatial frequencies (long wavelengths). The self-affine region follows a power law, $C(q) = q^{-\beta}$, which is a straight line in an ideal log-log PSD plot as displayed in Figure 13. The fractal dimension of the surface can be extracted using this power law. The fractal dimension is then

$$D = \frac{2n + 3 - \beta}{2} \tag{15}$$

where n is the dimension of the measurement, meaning 1 for a line-scan and 2 for a surface. The roll-off region is where the self-affinity of the surface breaks down, and will therefore not follow the same power law as the self-affine region does.[44]

In order to remain unbiased of the size and resolution of the measurements, the "Master PSD" can be calculated. PSD functions of individual measurements are stitched together to create a combined PSD which contains information about larger parts of the surface than the individual PSD functions. If measurements from different instruments is combined one can also remove much of the bias associated with each measuring instrument. The Master PSD can be calculated using a geometric mean with a weight function

$$C(q)^{\text{1D+}}_{\text{combined}} = \left[\prod_{i=1}^{M} (C_i(q)^{\text{1D+}})^{w_i(q)}\right]^{1/\sum_{i=1}^{M} w_i(q)} \tag{16}$$

where M is the number of PSD's to be combined and $w_i(q)$ is the weight function of the ith PSD, $C_i(q)^{\text{1D+}}$[42]. The weight function used in this study was a Hann function which decreases the weight of the PSD values of very low and very high spatial frequencies when combining the individual PSD's. These values are usually less accurate due to less information being present in the measurement at very low and very high spatial frequencies. Figure 14 shows the Hann window, also called a raised cosine function.

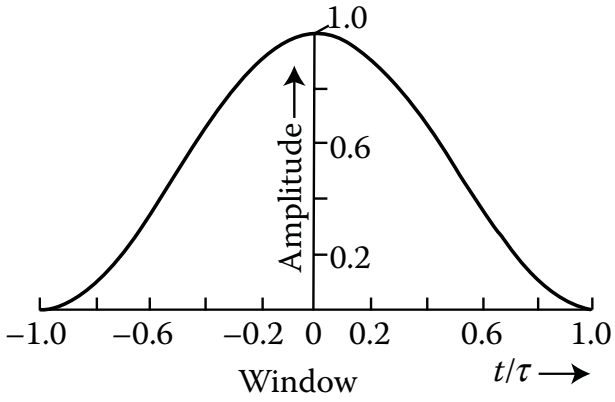

Figure 14: Graph of a Hann window or a raised cosine which will lower the weight of very low and high spatial frequencies[45].

The following equations were used to calculate the RMS roughness, h_{rms}, RMS slope, h'_{rms}, and RMS curvature h''_{rms} respectively

$$(h_{rms})^2 = \frac{1}{\pi}\int_0^\infty C(q)dq \tag{17}$$

$$(h'_{rms})^2 = \frac{1}{\pi}\int_0^\infty q^2C(q)dq \tag{18}$$

$$(h''_{rms})^2 = \frac{1}{\pi}\int_0^\infty q^4C(q)dq \tag{19}$$

These values use a different notation from the RMS roughness, slope and curvature in Section 2.3.3 to distinguish between the physical values and the ones calculated from the PSD.

The script used to calculate the master PSD and the RMS roughness, slope and curvature is given in Appendix B. Figure 15 illustrates the increased weighting of higher spatial frequencies for the RMS slope and RMS curvature.

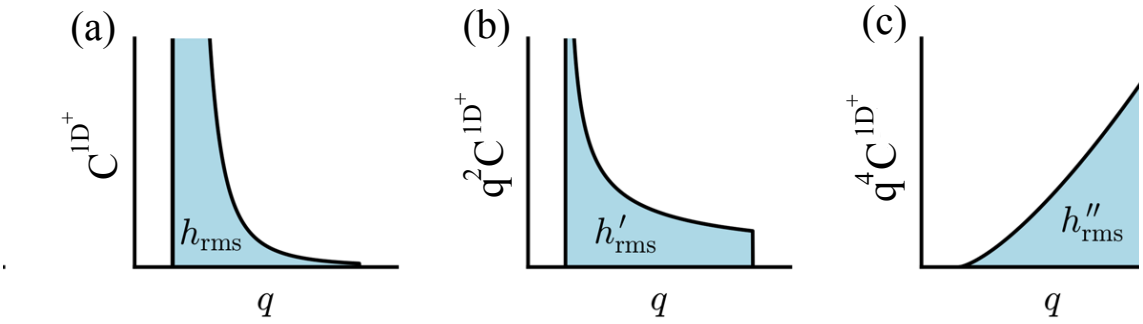

Figure 15: Visual representation of RMS roughness, slope and curvature calculated using the PSD. Figure (b) and (c) show an increasing weighting of the higher spatial frequencies. Amended from [26].

3.4 Statistical analysis

In order to review the effect of paint ingredients on the contact angle and surface roughness, linear regression analyses with multiple predictors were performed on the results. The significant predictors were chosen based on forward selection with a level of significance of 25%. Meaning there had to be at least a 75% chance of the predictor correlating with the response in order to enter the model. Forward selection is a type of stepwise regression where the optimal subset of predictors are added to the model[46]. Predictors which do not display high enough correlation with the response, in this case having p-values above 0.25, will not be added to the model. Cross-terms were also added to the model though they were manually removed if the individual terms included in the cross-terms were not themselves significant. For models which included two binders, the binder term was chosen to be a continuous predictor. For the relevant models, Silikopon EF had the value 0 and Epoxy had the value 1. All T-values and p-values of the model terms were recorded in addition to the R^2-values. An overview of all the regression analyses performed is given in Table 2.

Table 2: Overview of predictors and responses used in the regression models mentioned in this section, before forward selection was performed, and the sections in which the results and discussion of the models are presented. Samples with binders Epoxy and Silikopon EF are denoted EP and SP respectively.

Section with results	**Predictors**	**Responses**
Section 4.4	Binder, Additive, RMS curvature	Contact angle
	Binder, Additive, RMS slope	Contact angle
	Binder, Additive, RMS roughness	Contact angle
	RMS slope	RMS curvature
Section 4.5	Functionalisation, RMS curvature	Contact angle (EP)
	DE, Functionalisation	RMS curvature (EP)
Section 4.6	Binder, Additive, FDE	Contact angle
	Binder, Additive, FDE	RMS curvature
Section 4.7	Binder, Additive, FDE, Aerosil	Contact angle
	Binder, Additive, FDE, Aerosil	RMS curvature
Section 4.8	Additive, Λ, Ratio: FDE/total particles	Contact angle (SP)
	Additive, Λ, Ratio: FDE/total particles	RMS curvature (Sp)
	Additive, FDE, Nanosilica	RMS curvature (SP)
Section 4.9	Additive, FDE	Contact angle (Dowsil)
	Additive, FDE	RMS curvature (Dowsil)

First, the effect of the different roughness values on the water contact angle was explored. It was assumed that the particles affected the level of roughness the most and would therefore correlate, thus not including them in the model was essential. This assumption was tested in later regression analyses. Thus, the model comprised of binder type, whether or not there was an additive present and finally the roughness value. This was performed for each of the three roughness values h, h', and h". In addition to these three analyses, a regression analysis was performed to measure the level of correlation between the RMS slope and curvature. The RMS curvature was set as the response and the RMS slope as

the predictor. As these two values are both calculated from modified PSD functions, it was important to explore to what degree these two might correlate.

Then the effect of functionalising diatomaceous earth (FDE) was explored by doing a regression analysis of the samples with Silikopon EF binder, no additives and an increasing amount of either functionalised or non-functionalised diatomaceous earth as the predictors. In order to isolate the effect of roughness on the WCA, RMS curvature was also used as a predictor. Non-functionalised samples were represented by a 0 and functionalised by 1 in order to mimic a categorical predictor. A regression analysis was performed for both the WCA and the RMS curvature as responses in order to review what ingredients increased the WCA and what ingredients increased the roughness.

Paint samples with aerosil and no FDE at high Λ-values showed cracking and could therefore not be used in the regression analysis. Thus, an analysis of the type of binder, presence of the additive and amount of FDE as predictors was performed and the few samples with aerosil and no FDE that did not crack were excluded from the analysis. Both the WCA and the RMS curvature were used as responses.

The paint samples with both aerosil and FDE and high Λ-values did not crack and could therefore be analysed. This regression analysis used the type of binder, presence of the additive and the amount of FDE and aerosil as predictors in the model. The WCA and RMS curvature were the responses.

The effect of adding nanosilica to Silikopon EF binder with different amounts of additive and FDE was explored. The amount of additive, and the ratio of the amount of FDE to the total amount of particles (FDE and nanosilica) were used as predictors in a regression model and WCA and RMS curvature as responses. Also, a regression model with the amount of additive, FDE and nanosilica as predictors and RMS curvature as the response was performed in order to study the effect of nanosilica on the RMS roughness.

Since both the Silikopon EF binder and the Epoxy binder are slightly hydrophilic, a regression analysis with samples with a different binder, Dowsil, was also performed. The presence of the additive and the amount of FDE were used as predictors and WCA and RMS curvature as responses.

4 Results and discussion

This section will contain results from and discussions of the paint samples analysed. There will be some discussion concerning the size range of the RMS roughness, slope and curvature in order to understand the limitations of the microscopy methods used in this paper. All statistical analyses will be presented and discussed. The samples will be named as Binder_Additive_Particles_ Λ-value, as seen in Table 32.

4.1 Size range of roughness values and the limitations of the microscopy method

To understand and interpret the later results it is necessary to look at the size range of the captured roughness. The functions in which the roughness values are extracted by integration is displayed in this section. An example sample, SP_FDE_TP4_08, with relatively high roughness values is used to demonstrate the limitations of the microscopy method. The RMS roughness, h, calculated from Figure 16 is dominated by very small spatial frequencies. It peaks at a spatial frequency at around 6000 m^{-1} and no more contribution to the roughness value occurs at around 0.8×10^{-6} m^{-1}. The peak spatial frequency translates to a wavelength calculated to be around 1 mm.

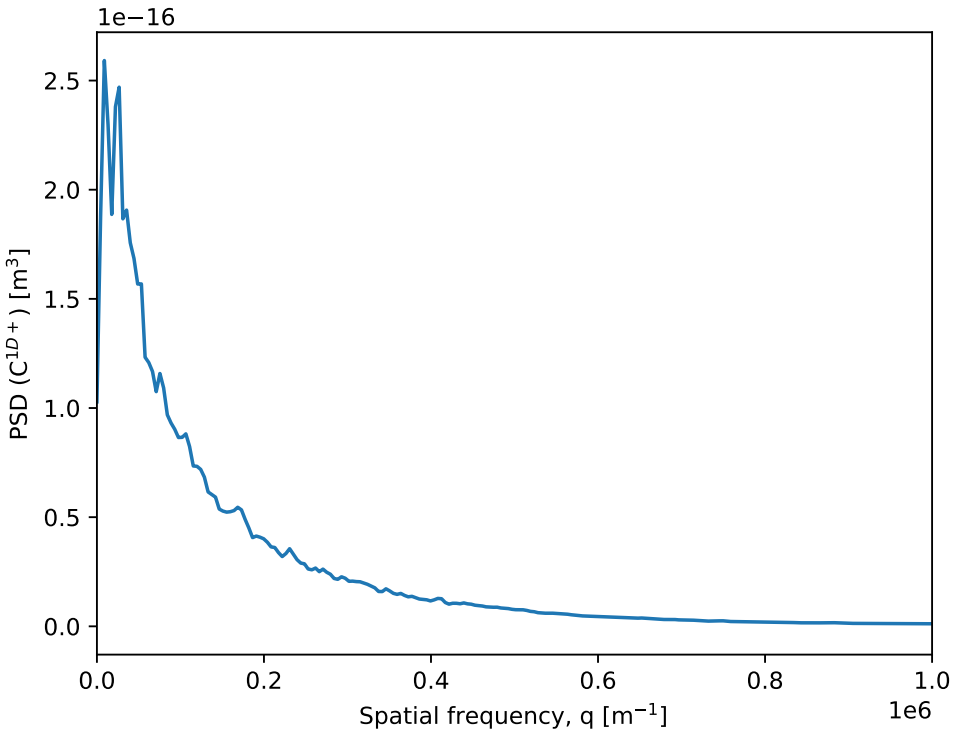

Figure 16: PSD function integrated to calculate RMS roughness of sample SP_FDE_TP4_08.

As expected, the contribution from higher spatial frequencies increases when calculating the RMS slope, as demonstrated in Figure 17. Here the spatial frequency peaks at around 40000 m^{-1}, translating to a wavelength of approximately 200 microns. Furthermore, this

function decreases more slowly than the function for RMS roughness. As the functions nears the limit of the spatial frequency domain, the contributions to the RMS slope is still significant.

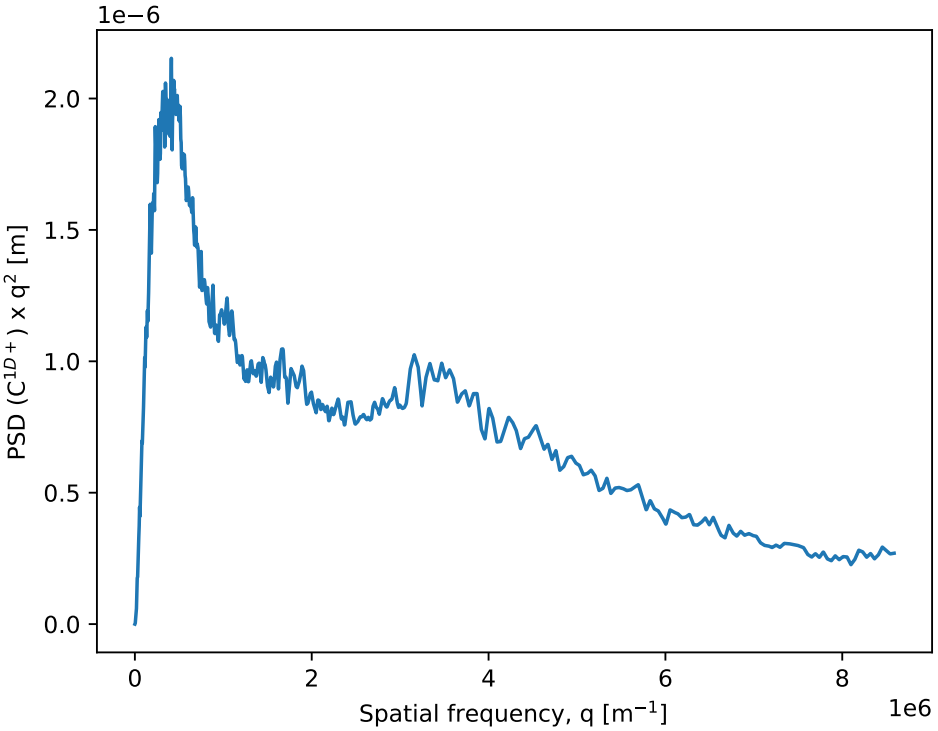

Figure 17: Modified PSD function integrated to calculate RMS slope of sample SP_FDE_TP4_08.

The curve used to calculate RMS curvature, Figure 18, has a low contribution to the RMS curvature at low spatial frequencies and increase steadily to a higher contribution at higher spatial frequencies. The curve peaks at the spatial frequency limit, around 8500000 m^{-1}, which corresponds to around 0.7 microns. This means that roughness smaller than 0.7 microns will not be detected using the current measuring techniques. This is one of the largest weaknesses of this study as very small-scaled roughness cannot be observed. An attempt was made in order to study the surface with an atomic force microscope (AFM) in order to explore the effect of smaller-scaled roughness. However, due to large wavelength roughness of the samples the data was dominated by noise. Therefore, when processing the data the PSD functions did not coincide with PSD functions of other measurements and could not be used.

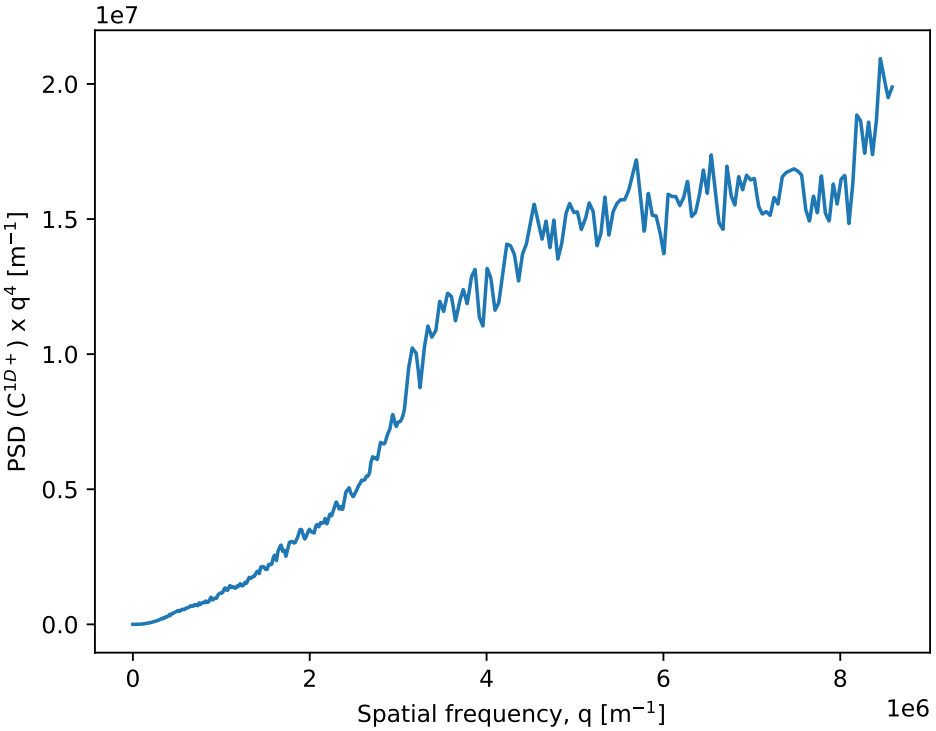

Figure 18: Modified PSD function integrated to calculate RMS curvature of sample SP_FDE_TP4_08.

4.2 The level of uncertainty in sample preparation and PSD calculations

Before performing statistical analysis it is important to discuss the uncertainties associated with the predictors and responses used. Every sample consists of a given weight percentage of each paint ingredient, but the samples will have varying degrees of viscosity due to different weight percentages of particles added. In order to prepare samples by draw down the formulation cannot be high in viscosity, which it often is for high Λ-values. To prevent this, Xylene is added to decrease viscosity allowing to do draw downs. This variability in viscosity might have an effect on the sample's hydrophobicity and roughness values. As the amount of xylene added to the paint might affect the wetting of the particles by the binder and the drying time, its presence will most likely affect the surface formation process.

Another factor of uncertainty to be taken into consideration is the PSD calculations as the PSD function will most likely vary based on where on the sample a measurement is performed. For sample SP_FDE_TP4_04 five measurements at different areas of the surface were performed for all the magnification. For each of the five measurements RMS roughness, slope and curvature was calculated. In Table 3 the mean, standard deviation (SD) and coefficient of variance (CV) of each of the three values are displayed. The CV is defined as the ratio of the SD over the mean and gives an indication of the degree of variation in the relation to the mean. The CV is relatively low, but significant enough to affect the regression models to some degree. However, due to time restrictions measurements were only performed at one spot on the surface.

Table 3: Overview of the mean, standard deviation and coefficient of variance of roughness values for sample SP_FDE_TP4_04.

Roughness value	**Mean**	**Standard deviation**	**Coefficient of variance**
RMS roughness	0.541 μm	0.0430 μm	7.95%
RMS slope	1.41	0.0863	6.12%
RMS curvature	5.57 Mm	0.464 Mm	8.33%

4.3 The binders and their level of hydrophobicity

In order to get a better understanding of the binders used in the main analysis, their WCA's are presented in Table 4. The table includes the binders Silikopon EF and Epoxy both with and without the presence of an additive. The Silikopon EF binder is slightly hydrophilic with a WCA of 86.0°. Adding the additive increases the WCA by approximately 10°. The Epoxy binder is hydrophilic, displaying a WCA of only 64.9°. However, in the presence of an additive the WCA increases almost 30°. Thus, with an additive, both of the binders show an increase in hydrophobic behaviours. Though the additive had a higher impact in the epoxy binder, it still had a significant effect on the Silikopon EF binder.

The RMS curvature of the samples are also presented in Table 4. There is an increase in RMS curvature for both binders when the additive is present. Therefore, the interaction between the binder and the additive did increase the surface roughness of the samples. Notably, the Epoxy binder has a higher increase in RMS curvature which might indicate the Silikopon EF binder masks the surface roughness more compared to the Epoxy binder. It might be assumed that the Silikopon EF binder has a better levelling ability. With the methods presented in this paper it is not possible to distinguish between hydrophobicity increased by chemical composition or by surface roughness.

Table 4: An overview of the water contact angles (WCA) and RMS curvature (h″) of the binders used in the main analysis with and without the additive.

Sample	**WCA** [°]	**h″[Mm]**
Silkopon EF no additive	86.0	0.0305
Silkopon EF with additive	96.3	0.125
Epoxy no additive	64.9	0.0259
Epoxy with additive	93.2	0.822

4.4 The effect of additive, binder and roughness values on the contact angle

Assuming the particles added to the binder account for most of the surface roughness, one can model the effect of the roughness values by linear regression using only the additive, binder and the roughness value of interest as predictors for the WCA. Some of the roughness might be due to the presence of the additive, but it is assumed that the added particles dominate the increase in roughness. Thus one can for the most part isolate the effect of the level of roughness by taking these factors into account in the regression analysis. An overview of the predictors and responses used in the regression models in

this section is presented in Table 5. Since only two binders were used, the type of binder was added to the model as a continuous predictor by representing Silikopon EF as 0 and Epoxy as 1. The samples used in this analysis and WCA and roughness values are given in Table 32 and Table 33. These samples contain varying degrees of FDE and for some of the samples with Λ-values there is aerosil present as well.

Table 5: Overview of predictors and responses used in the regression models displayed in this section before forward selection was performed.

Responses	**Predictors**
Contact angle	Binder, Additive, RMS curvature
Contact angle	Binder, Additive, RMS slope
Contact angle	Binder, Additive, RMS roughness

The results of this analysis are presented in Table 6. The additive clearly shows a positive effect on the WCA as the T-value is positive and the p-value is far below the usual level of significance, 5%. The binder also affected the WCA. Switching from Silikopon EF to Epoxy had a negative impact on the WCA, as the T-value of the binder term is negative and the p-value is much lower than 5%. Therefore, for this combination of ingredients, Silikopon EF works best to increase the WCA. The RMS curvature also had a significant effect with a high and positive T-value and a very small p-value. Thus confirming the importance of roughness to increase hydrophobicity. The regression analysis is considered to be a good model as the R^2-value for the model is 68.9%, which is acceptable when taking the uncertainties of sample preparation and roughness from PSD calculations into consideration.

Table 6: The effect of additive, binder and RMS curvature on the contact angle. The R^2-value for the model is 68.9%.

Term	**T-value**	**p-value**
Binder	-4.92	1.51×10^{-5}
Additive	3.42	1.46×10^{-3}
Curvature	5.73	1.15×10^{-6}

Figure 19 displays a fitted line plot of WCA vs. RMS curvature. The values are grouped by the presence of the additive and the type of binder in order to visualise the data represented by the model in Table 6. As in the regression model, the WCA increases when the curvature is increased. The samples with Silikopon EF has for the most part the highest WCA's in comparison to their RMS curvatures, but the value with the highest WCA and RMS curvature is a sample with Epoxy binder. Additionally, there is a very high level of variance for samples with Epoxy binder, no additive and high levels of RMS curvature.

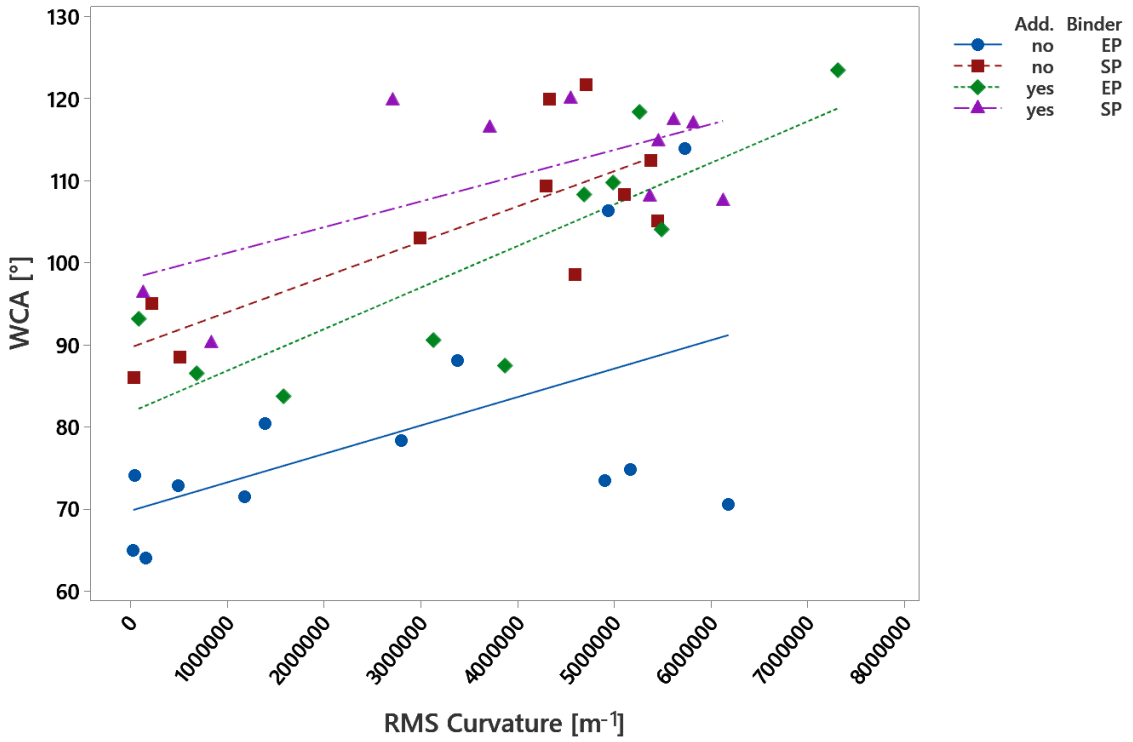

Figure 19: Fitted line plot of WCA vs. RMS curvature grouped by the presence of the additive and type of binder.

In Table 7 a similar regression model is created with the RMS slope as a predictor instead of the RMS curvature. The R^2-value of the model is 55.6% which is lower than the model presented in Table 6. There are similar correlations between the models since the additive, the type of binder and the RMS slope was added to the model by forward selection. However, the model's lower R^2-value signifies a higher level of variation compared to the model in Table 6.

The sample results are represented in Figure 20 by a fitted line plot. The data is grouped by the presence of the additive and the type of binder. Though the fitted lines indicate similar relationships between the groups as seen in Figure 19, there are less linear behaviour for some groups. For samples with Silikopon EF and additive, most samples show high WCA's and the RMS slope does not seem to affect the WCA much apart from one sample, highlighted by the black circle, which show low WCA and low RMS slope. Samples with Silikopon EF binder and no additive does follow a more linear relationship, but have high variations for high WCA's. The same result can be seen for the samples with the Epoxy binder. This might mean that when the samples reach higher WCA's, the RMS slope correlates less.

Table 7: The effect of additive, binder and RMS slope on the contact angle. The R^2-value for the model is 55.6%.

Term	**T-value**	**p-value**
Binder	-4.80	2.26×10^{-5}
Additive	2.91	5.83×10^{-3}
Slope	3.37	1.65×10^{-3}

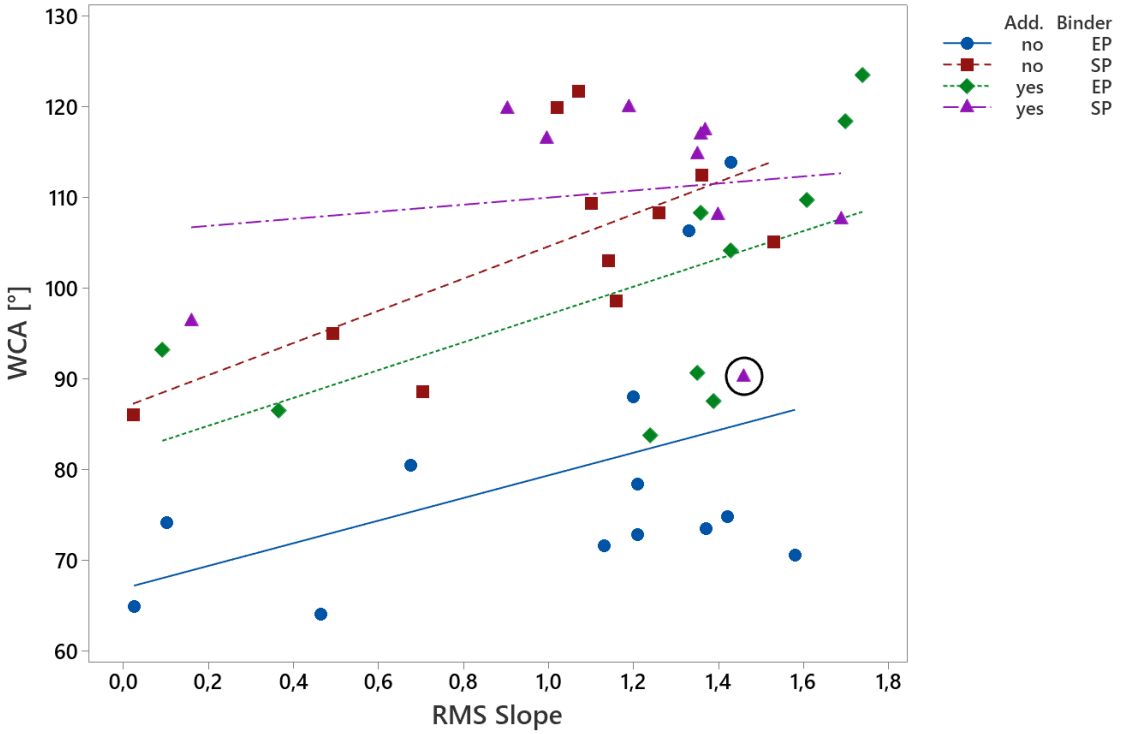

Figure 20: Fitted line plot of WCA vs. RMS slope grouped by the presence of additive and type of binder.

By switching the predictor to RMS roughness, the model worsens again. The regression model includes the values given in Table 8, but with an extremely low R^2-value of 20.8%. This could either be due to high variations in the values or a lack of predictors to describe the change in the response. Since the RMS roughness term in Table 8 has a p-value of 0.123, there is some correlation with the WCA and it has been included in the model by forward selection, but it is quite high, meaning there is a likelihood of the correlation being due to random variation. Figure 21 displays a fitted line plot of WCA vs. RMS curvature. The values are grouped by the presence of the additive and the type of binder in order to visualise the data represented by the model in Table 8. Apart from two outliers, most of the values in the fitted line plots seems to be variations around a mean. The RMS roughness is therefore not a good predictor for WCA's considering the limitations in the resolution of the microscope techniques.

Table 8: The effect of additive, binder and RMS roughness on the water contact angle. The R^2-value for the model is 20.8%.

Term	**T-value**	**p-value**
Binder	-1.97	6.18×10^{-2}
Roughness	1.61	0.123

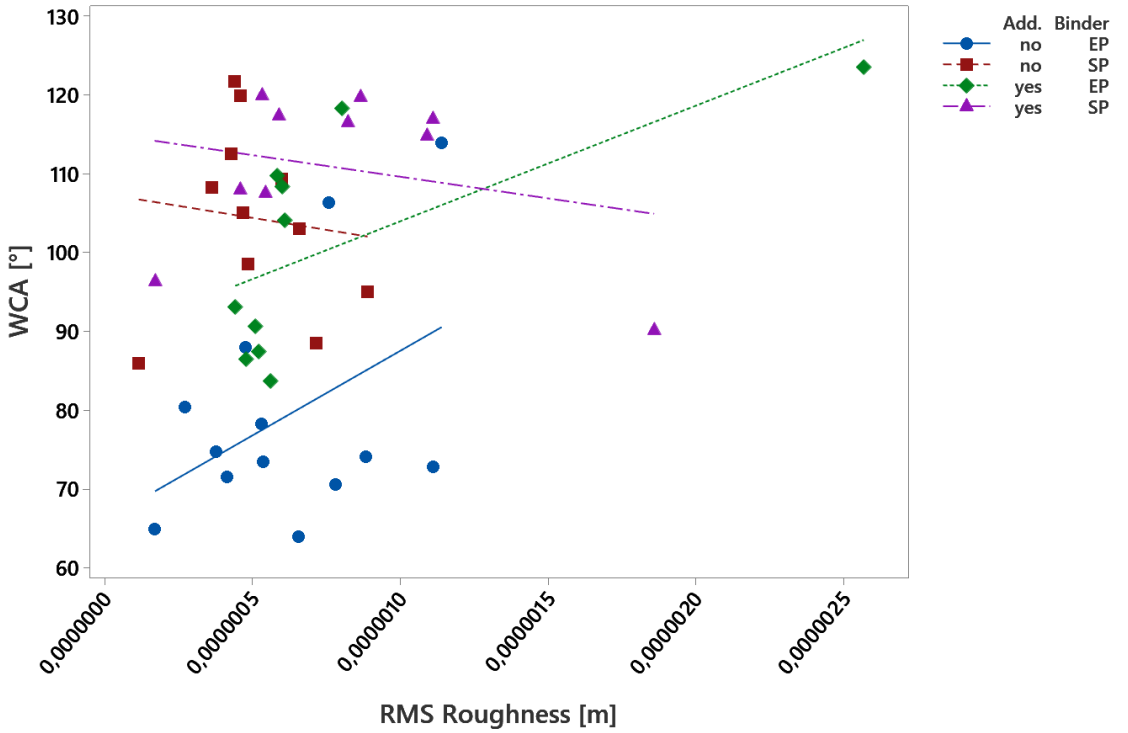

Figure 21: Fitted line plot of WCA vs. RMS roughness grouped by the presence of additive and type of binder.

By modelling the effect of roughness using the three different roughness values one gets a better understanding of which size ranges are relevant for a hydrophobic surface behaviour. The roughness values that include low spatial frequencies is dominated by a level of roughness which is too large to affect the small droplets used to measure the WCA and consequently the level of hydrophobicity of the paint samples. The RMS slope is significant in the model shown in Table 7, but the R^2-value of the model is low. Additionally, there is a high level of correlation between the RMS slope and curvature, shown in Table 9.

Correlations between curvature and slope, demonstrated by the small p-value in the linear regression model displayed in Table 9, might be due to the limited size range the microscopic technique encompasses. Meaning, the PSD functions the RMS slope and RMS curvature is integrated from consist of too similar-sized roughness features for us to differentiate between them effectively. Then the difference in the two values is only due to the increased weight of large scale roughness of the RMS slope, such as the roughness with wavelengths around 1 mm, which does not affect the WCA. This may explain why the RMS slope is significant in Table 7, but the model has a lower R^2-value than the model in Table 6 using the RMS curvature as a predictor instead.

Table 9: The effect of RMS slope on RMS curvature. The R^2-value for the model is 60.3%.

Term	**T-value**	**p-value**
Slope	5.73	5.69×10^{-10}

An effort was put in this section to highlight that the RMS roughness and RMS slope will not provide any significant or useful correlation in further analyses. RMS roughness is dominated by a roughness scale which is too large to affect the hydrophobicity of the

surface. This is in accordance with literature as RMS roughness values of approximately 1 nanometre is used to correlate hydrophobicity whereas RMS roughness values calculated in this study is around 1 micrometre[47]. The RMS slope values in this study correlate too much with the RMS curvature while also showing more variations when correlating it to the WCA. The scale of roughness represented by RMS roughness and RMS slope in this study is on the millimetre scale and higher micrometre scale respectively, as discussed in Section 4.1, but should be on the lower micrometre scale. Ideally, these two values would represent a smaller scale of roughness which is as large as possible while still affecting the WCA. Additionally, using measuring techniques with higher resolution, such as the AFM, would result in RMS curvature values representing a smaller scale of roughness than RMS roughness and slope, preferably in the nanometre regime. This would allow the model to differentiate between micro-scaled and nano-scaled roughness which, according to literature, are both needed in order to achieve a high degree of hydrophobicity, namely superhydrophobicity.

4.5 The effect of functionalising diatomaceous earth

The diatomaceous earth was hydrophobically functionalised in order to try to increase the chemical hydrophobicity of the surface along with the surface roughness. A sample of tape with FDE showed WCA's of slightly lower than 140°. Functionalisation of DE is assumed to be the most effective if some of the particles are exposed to the surface and not fully wetted by the binder. Therefore an analysis on the effect of non-functionalised DE (NFDE) vs. FDE on the WCA was conducted. The samples in this analysis used the Epoxy binder. The funtionalisation's effect on the RMS curvature was also investigated. SEM images of NFDE and FDE are displayed in Figure 22a and Figure 22b, respectively. The FDE particle seems to have more fringes at the edges and are therefore less rounded compared to the NFDE particle. They are also smaller as their original structure was most likely damaged during functionalisation.

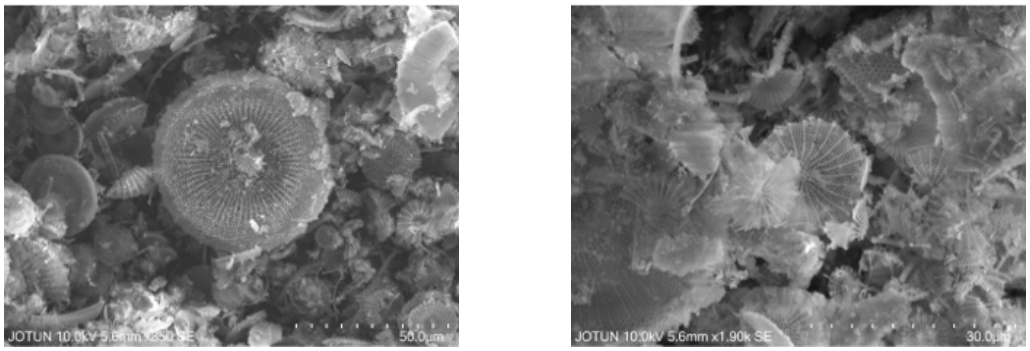

(a) SEM picture of non-functionalised DE. (b) SEM picture of FDE.

Figure 22: SEM pictures of NFDE and FDE.

As there are complex processes which determine the structure of surfaces, using a more hydrophobic particle might affect the way in which the particle interacts with the binder and positions itself on the surface and whether or not it is wetted by the binder. In this section diatomaceous earth (DE) will be used to refer to both NFDE and FDE. The samples in this analysis did not contain an additive. An overview of predictors and responses used in this section is displayed in Table 10. The samples used and their paint ingredients are all presented in Table 11.

Table 10: Overview of predictors and responses used in the regression models displayed in this section before forward selection was performed.

Responses	**Predictors**
Contact angle	Functionalisation, RMS curvature
RMS curvature	DE, Functionalisation

Table 11: Overview of predictors and responses used in the regression models displayed in this section before forward selection was performed.

Sample	**Functionalised**	**DE** [w%]	Λ	**WCA** [°]	**h"** [Mm^{-1}]
EP_00	-	0.00	0.00	64.9	0.0259
EP_DE_04	no	17	0.40	62.0	0.0461
EP_DE_06	no	24	0.60	58.7	2.20
EP_DE_08	no	31	0.80	81.2	6.08
EP_DE_10	no	38	1.00	97.2	7.70
EP_DE_12	no	44	1.20	85.3	7.69
EP_FDE_04	yes	17	0.40	74.1	0.0455
EP_FDE_06	yes	24	0.64	72.8	0.490
EP_FDE_08	yes	31	0.77	88.1	3.38
EP_FDE_10	yes	38	1.00	106.4	4.94
EP_FDE_12	yes	44	1.20	113.9	5.73

In Table 12 the results from the analysis of the effect of functionalising DE on the WCA is displayed. In order to mimic a categorical predictor, the NFDE was set as 0 and the FDE as 1. Since the samples with the same Λ-values contain the same amounts of DE, RMS curvature was used as a predictor instead of the amount of DE. This decision was made to try to differentiate between the effect of roughness on the WCA and the effect of the difference in chemistry, here the functionalisation. This is a simplified model as there will most likely be varying surface roughness due to the interaction between the functionalised and non-functionalised particles with the binder.

As expected, using FDE and increasing the RMS curvature both have a very significant effect on the WCA. The R^2-value for the model is 72.7% which is an acceptable value and shows a clear correlation between the predictors and the response without being dominated by variance. The effect of FDE while taking into consideration the effect of the RMS curvature supports the idea that some of the FDE particles are exposed at the surface, not coated by the binder or covered by a thinner layer of the binder, allowing nanoroughness to define the surface. Therefore, it can be assumed that there is some difference in the level of wetting between NFDE and FDE. Otherwise, more correlation between the two predictors, functionalisation and RMS curvature could be expected, making one of them redundant. As both are significant, there has to be an increase in the WCA's due to higher chemical hydrophobicity or a level of roughness which the methods used in this study could not detect.

Table 12: The effect of functionalising diatomaceous earth and RMS curvature on the water contact angle. The R^2-value for the model is 72.7%.

Term	T-value	p-value
Functionalisation	4.06	2.84×10^{-3}
Curvature	6.27	1.45×10^{-4}

Figure 23 shows a fitted line plot of the data represented in the model in Table 12. The values are grouped by whether or not the DE is functionalised. No new information is gained by this fitted line plot as the WCA increases with RMS curvature and samples with FDE show overall higher WCA's compared to the samples with NFDE.

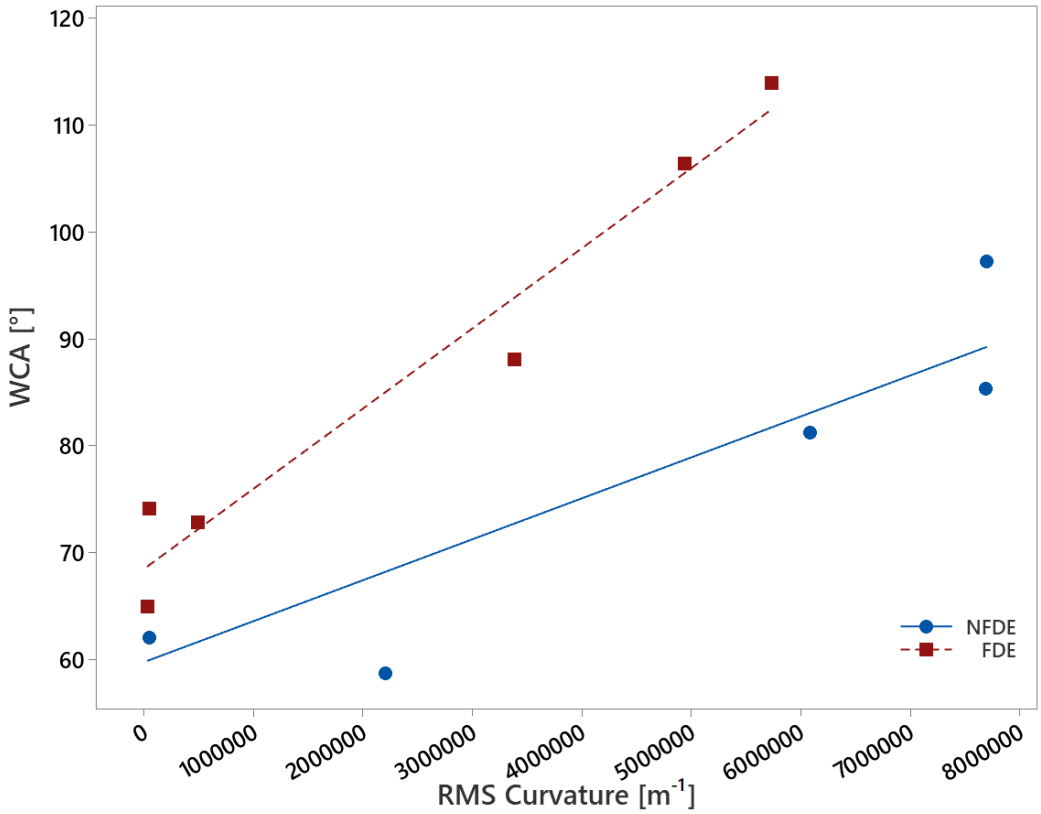

Figure 23: Fitted line plot of WCA vs. RMS curvature grouped by whether the DE is functionalised or not.

In order to explore the effect functionalisation of DE had on the roughness of the surface, a regression analysis with the amount of DE and the functionalisation as predictors and RMS curvature as the response was performed. The results are displayed in Table 13. Again the amount of DE is significant, as an increase in diatomaceous earth, both functionalised and non-functionalised, directly increases the surface roughness. The functionalisation term has a negative T-value and a p-value of 0.115. This is larger than the usual limit of 0.05, but was lower than 0.25 and was thus added by forward selection.

Table 13: The effect of functionalising diatomaceous earth on the RMS curvature. The R^2-value for the model is 80.8%.

Term	T-value	p-value
DE	5.89	2.31×10^{-4}
Functionalisation	-1.75	0.115

To examine this result, a fitted line plot is displayed in Figure 24 which shows the relationship between RMS curvature and the weight percentage of DE grouped by whether the DE is functionalised or not. For all weight percentages of DE above 20%, the samples with NFDE have higher RMS curvature values than the samples with FDE, yet displaying higher levels of hydrophobicity. This could be due to an increase in the chemical hydrophobicity of the surface due to the functionalisation of DE. The decrease in RMS curvature might be due to DE particles being damaged during functionalisation as seen in Figure 22. A different reason might be a higher level of nanoroughness which the methods in this study is not able to detect. The binder might be covering the NFDE, creating a slightly higher roughness on the micro-level, but also levelling out the nanoroughness of the DE particles. This might be due to the different wetting behaviours of the NFDE compared to the FDE as mentioned before. Due to the higher level of hydrophobicity of the FDE, the binder might be less inclined to wet the particles at the surface compared to the NFDE. For confirmation, further work would need to be done with measurements techniques with higher resolutions.

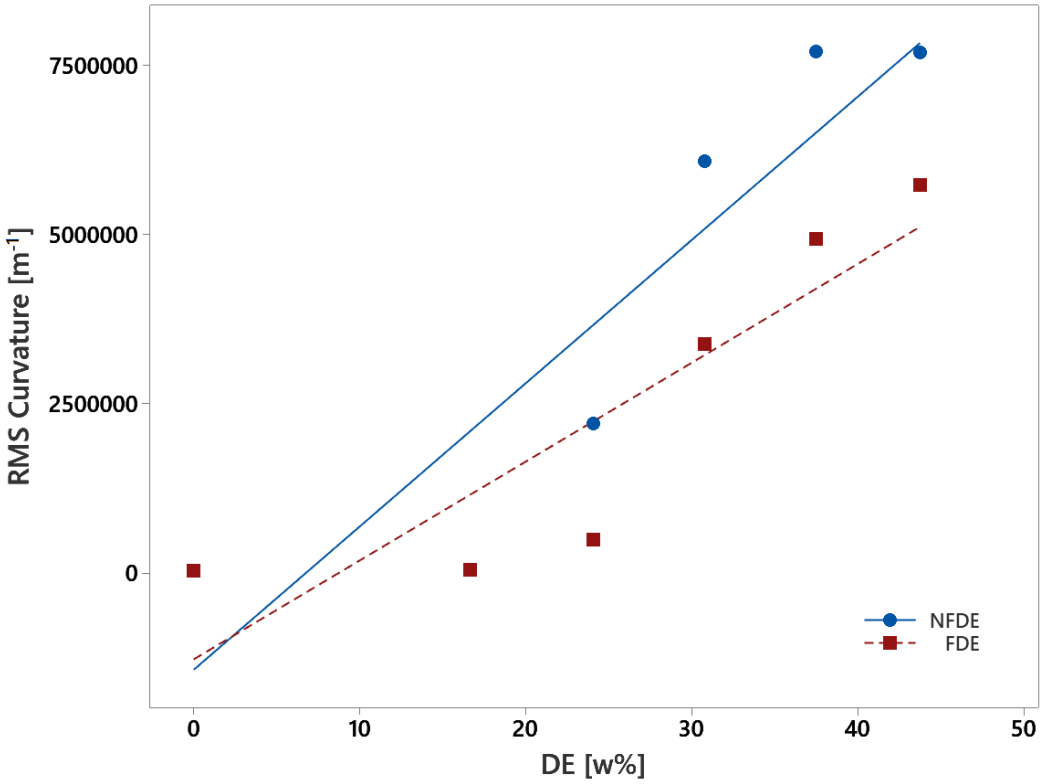

Figure 24: Fitted line plot of RMS curvature vs. weight percentage of DE grouped by whether the DE is functionalised or not.

4.6 The effect of binder, additive and amount of FDE

This section explores the effect of the type of binder, the presence of an additive and the amount of FDE on the water contact angle and the RMS curvature. Table 14 displays the responses and predictors used in the regression analyses before forward selection was performed. An overview of paint ingredients, WCA and RMS curvature results are given in Table 15.

Table 14: Overview of predictors and responses used in the regression models displayed in this section before forward selection was performed.

Responses	**Predictors**
Contact angle	Binder, Additive, FDE
RMS curvature	Binder, Additive, FDE

Table 15: An overview of the samples and their results used in the statistical analysis of binder, additive and amount of FDE. The binder used is denoted in sample names as SP for Silikopon EF and EP for Epoxy.

Sample	**TP [w%]**	**FDE [w%]**	**Λ**	**WCA [°]**	**h" [Mm^{-1}]**
SP_00	0.00	0.00	0.00	86.0	0.0305
SP_FDE_04	0.00	21	0.40	95.0	0.214
SP_FDE_06	0.00	30	0.64	98.5	4.59
SP_FDE_08	0.00	35	0.77	109	4.29
SP_FDE_10	0.00	45	1.0	120	4.33
SP_FDE_12	0.00	50	1.2	122	4.71
SP_TP4_00	4.0	0.00	0.00	96.3	0.125
SP_FDE_TP4_04	4.0	19	0.40	90.2	0.834
SP_FDE_TP4_06	4.0	27	0.60	107	6.13
SP_FDE_TP4_08	4.0	35	0.80	108	5.37
SP_FDE_TP4_10	4.0	42	1.0	118	5.62
SP_FDE_TP4_12	4.0	48	1.2	117	5.82
EP_00	0.00	0.00	0.00	64.9	0.0259
EP_FDE_04	0.00	17	0.40	74.1	0.0455
EP_FDE_06	0.00	24	0.60	72.8	0.490
EP_FDE_08	0.00	31	0.80	88.1	3.38
EP_FDE_10	0.00	38	1.0	106	4.94
EP_FDE_12	0.00	44	1.2	114	5.73
EP_TP4_00	3.8	0.00	0.00	93.2	0.0822
EP_FDE_TP4_04	3.8	16	0.40	86.5	0.685
EP_FDE_TP4_06	3.8	23	0.60	83.7	1.58
EP_FDE_TP4_08	3.8	30	0.80	110	4.99
EP_FDE_TP4_10	3.8	36	1.0	118	5.26
EP_FDE_TP4_11	3.8	42	1.1	124	7.32

Table 16 displays the results from the regression analysis with WCA as the response. The binder has a negative T-value and a p-value of less than 5%. Silikopon EF therefore seems to be the most promising binder to increase hydrophobicity. The additive as well has a significant effect on the WCA with a positive T-value meaning its presence is favourable.

The FDE also has a positive T-value and a very small p-value, far below 5%. This is most likely due to its contribution to the surface roughness.

Table 16: The effect of binder, additive and amount of FDE on the water contact angle. The R^2-value for the model is 75.3%.

Term	**T-value**	**p-value**
Binder	-2.11	0.0484
Additive	2.47	0.0230
FDE	4.04	6.93×10^{-4}
Binder× FDE	1.35	0.194

A term of interest in this model is the cross term, Binder×FDE having a positive T-value and a p-value of 0.194. This means the combination of Epoxy binder and FDE increases the WCA. The p-value was included in the model as it was less than 0.25, but it is still quite high compared to the usual significance level of 0.05. It is however an interesting result, and its occurrence is most likely due to the high WCA's observed for Epoxy with high amounts of FDE and the presence of an additive. Sample EP_FDE_TP4_11 has a WCA of 124, presented in Table 15, which was the highest WCA of all the samples used in this model. This result highlights the unpredictable behaviour of paint formulations. Though the results thus far clearly favour Silikopon EF as the superior binder to create hydrophobic coatings, a single Epoxy based coating shows the best results. Still, the R^2-value for the model is 75.3% which shows clear correlation within the uncertainties of the model.

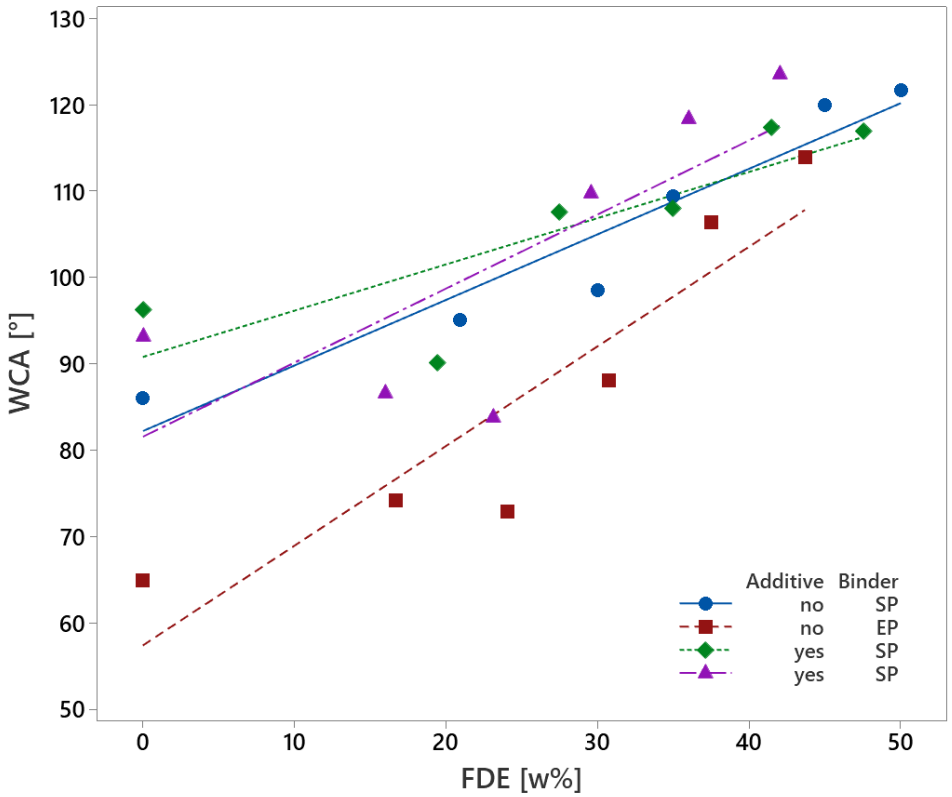

Figure 25: Fitted line plot of WCA vs. weight percentage of FDE grouped by the presence of additive and the type of binder.

In Figure 25, a fitted line plot of WCA vs. the weight percentage of FDE is displayed. The values are grouped by the presence of the additive and the type of binder in order to visualise the data represented by the model in Table 16. All the values follow a mostly linear trend. From the regression results one would expect that the highest WCA's correspond to samples which have a combination of Silikopon EF binder and the additive. However, the highest WCA's in the plot clearly belongs to samples with Epoxy and additive and samples with Silikopon EF and no additive. Additionally, the samples with Epoxy and no additive show a much higher increase in WCA with the increase in FDE, which agrees with the Binder×FDE term in Table 16. The regression model favours the combination of Silikopon EF binder and the presence of the additive due to the large effect on WCA for low levels of FDE, but when increasing the amount of FDE in the samples, the importance of Silikopon EF and the additive might diminish.

In Table 17, the results from the regression analysis with RMS curvature as the response are displayed. As expected, WCA increases with the amount of FDE. The term has a positive T-value and an extremely small p-value which corresponds with earlier results. In addition to the FDE, the additive also has a positive effect on the RMS curvature. The additive did have an effect on the RMS curvature, as discussed in Section 4.3.

Table 17: The effect of binder, additive and amount of FDE on RMS curvature. The R^2-value for the model is 77.4%.

Term	**T-value**	**p-value**
Additive	2.16	0.0425
FDE	8.29	4.64×10^{-8}

Figure 26 displays a fitted line plot of RMS curvature vs. the weight percentage of FDE. The values are grouped by the presence of the additive and the type of binder in order to visualise the data represented by the model in Table 17. As expected from the regression results, the highest RMS curvature values belong to samples with the additive and a high weight percentage of FDE. The effect of the presence of the additive is not noticeable when no FDE is present, but seems to increase with the increase of FDE.

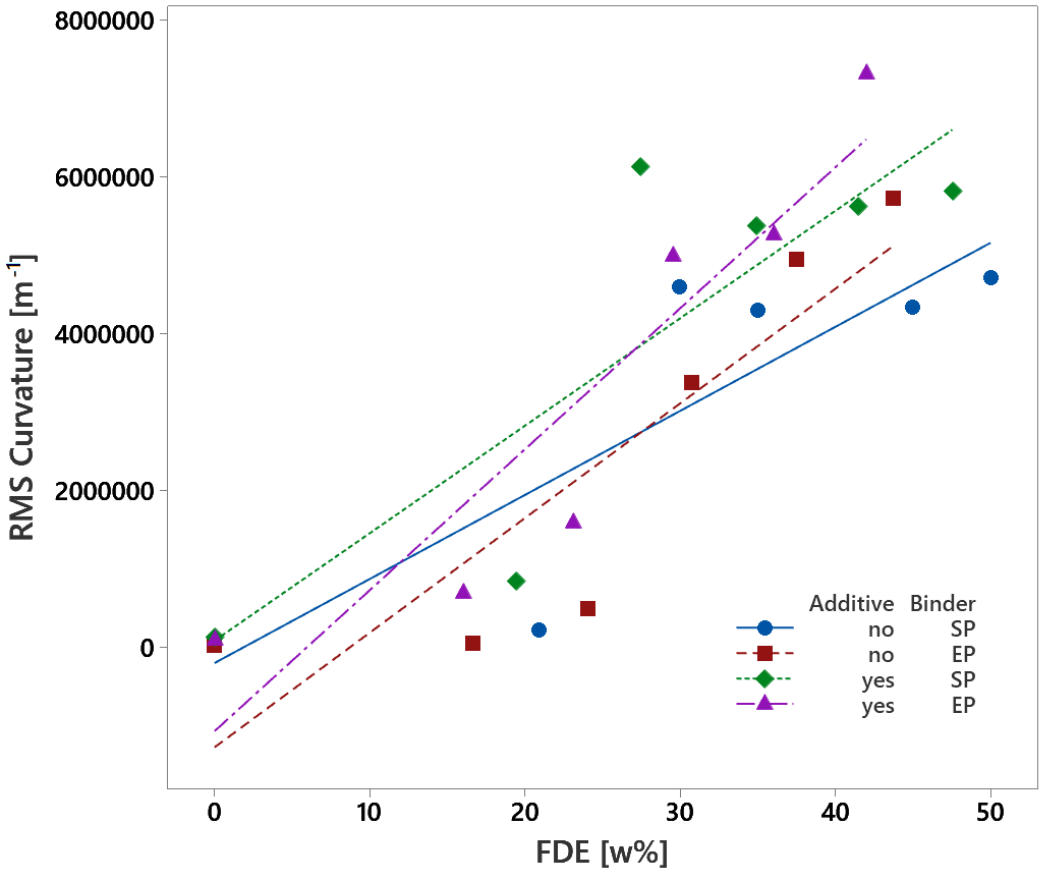

Figure 26: Fitted line plot of RMS curvature vs. weight percentage of FDE grouped by the presence of additive and the type of binder.

In Figure 25 samples with Silikopon EF binder and no additive show high WCA's for high levels of FDE. In Figure 26 samples with Silikopon EF binder and no additive show low values for RMS curvature for high levels of FDE. So the effect of the presence of an additive on the WCA and RMS curvature is interesting. As discussed in Section 4.4 there is a high level of correlation between the WCA and the RMS curvature. There are mainly two reasons as to why lower levels of RMS curvature might lead to high levels of WCA. First, there might be a lower scale of roughness which the methods used in this study do not detect. Second, the additive might affect how many particles of FDE are exposed at the surface, decreasing the chemical hydrophobicity of the surface. By not adding the additive, the binder might interact with the particles in a way which allows for the FDE particles' lower level of roughness to define the surface more than for samples with the additive. The difference in the RMS curvature might be due the additive wetting the particles with a thicker layer of binder, increasing the microroughness slightly, but reducing sub-microroughness. This seems to be only relevant for the samples with Silikopon EF binder as samples with Epoxy binder show the expected trend of high RMS curvature resulting in high WCA's.

4.7 The effect of binder, additive, amount of FDE and aerosil for high Λ-values

Although the samples with only aerosil had the tendency to crack for high Λ-values, the samples with high Λ-values and a combination of FDE and aerosil showed an intact surface. Thus regression analyses to explore the effect of the type of binder, the presence of an additive, the amount of FDE and aerosil at high Λ-values were performed with WCA and RMS curvature as responses. Table 18 displays all the predictors and responses used in the analyses in this section before forward selection was performed. All individual samples used in the regression models and their paint ingredients and WCA and RMS curvature results are given in Table 19.

Table 18: Overview of predictors and responses used in the regression models displayed in this section before forward selection was performed.

Responses	**Predictors**
Contact angle	Binder, Additive, FDE, Aerosil
RMS curvature	Binder, Additive, FDE, Aerosil

Table 19: An overview of the samples and their results used in the statistical analysis of FDE and aerosil samples with high Λ-values. The binder used is denoted in sample names as SP for Silikopon EF and EP for Epoxy.

Sample	**TP** [w%]	**FDE** [w%]	**Aerosil** [w%]	Λ	**WCA** [°]	**h"** [$\mathbf{Mm^{-1}}$]
SP_FDE9_AE_10	0.00	38	4.2	1.0	108	3.94
SP_FDE4_AE_10	0.00	33	8.2	1.0	105	4.29
SP_FDE2_AE_10	0.00	26	13	1.0	103	2.40
SP_FDE4_AE_12	0.00	37	9.2	1.2	113	4.17
SP_FDE9_AE_TP4_10	4.1	36	4.0	1.0	115	4.26
SP_FDE4_AE_TP4_1P	4.2	32	7.9	1.0	120	3.52
SP_FDE2_AE_TP4_10	4.1	25	12	1.0	120	2.13
SP_FDE4_AE_TP4_12	4.0	36	8.8	1.2	116	2.87
EP_FDE9_AE_10	0.00	34	3.8	1.0	74.8	4.13
EP_FDE4_AE_10	0.00	29	7.4	1.0	73.5	3.84
EP_FDE2_AE_10	0.00	23	12	1.0	78.4	2.33
EP_FDE4_AE_12	0.00	34	8.5	1.2	70.6	4.87
EP_FDE9_AE_TP4_10	2.6	33	3.7	1.0	108	3.69
EP_FDE4_AE_TP4_10	2.7	29	7.2	1.0	87.5	3.16
EP_FDE2_AE_TP4_10	3.0	22	11	1.0	90.6	2.57
EP_FDE4_AE_TP4_12	2.6	33	8.3	1.2	104	4.28

The results with WCA as the response are displayed in Table 20. The model has a high R^2-value of 81.8%. Noticeably, the amounts of FDE and aerosil do not seem to have an effect on the WCA as they were not added to the model by forward selection. This was unexpected as FDE has been crucial in increasing the RMS curvature and therefore the WCA in other analyses. Additionally, aerosil has a high hydrophobicity and adding it to the tape, displayed later in this study in Section 4.11, increased the WCA to around

140°. Combining FDE with aerosil and the binder seems to diminish the aerosil's effect on the WCA. It might be assumed that this happens due to it being wetted by the binder and thus not being exposed at the surface. The high Λ-values should have allowed the aerosil not to be fully wetted by the binder, but this seems not to be the case. This should be further studied by doing wetting experiments to determine the true critical particle concentration for Λ=1.

Table 20: The effect of binder, additive and amount of FDE and aerosil for high Λ-values on the water contact angle. The R^2-value for the model is 81.8%.

Term	**T-value**	**p-value**
Binder	-5.80	6.15×10^{-5}
Additive	3.76	2.37×10^{-3}

As expected from previous results, both the binder and the additive effects the WCA. The negative T-value of the binder term implies the Silikopon EF binder is more successful in increasing the WCA than the Epoxy binder. The positive T-value of the additive, again, confirms its presence increases the WCA. In Table 19 the amounts of FDE, aerosil and additive in each sample and the resulting WCA and RMS curvature for each sample are displayed. By comparing the samples with and without the additive one can observe the effect it has on the WCA. For the Silikopon EF binder, adding the additive increases the WCA by around 10-15°, which approximately corresponds to the increase observed in Section 4.3. Adding an additive to the samples with the Epoxy binder increases the WCA by anywhere between 10-30°. This corresponds with results in Section 4.6, where the additive was more important to increase the WCA for samples with Epoxy binder than with Silikopon EF.

Figure 27 and Figure 28 display fitted line plots for samples with a combination of aerosil and FDE and high Λ-values of WCA vs. weight percentage of FDE and WCA vs. weight percentage of aerosil respectively. The values are grouped by the presence of the additive and the type of binder. The increase in WCA for samples with Silikopon EF corresponds with the results in Table 20. The presence of an additive also increases the WCA overall. Samples with Silikopon EF binder are less affected by the variations in amount of FDE and aerosil. Samples with the additive and Epoxy binder work better with only FDE, as seen in Section 4.6, than a combination between FDE and aerosil. Finally, samples with no additive and Epoxy binder show only hydrophilic tendencies, even though both FDE and aerosil are hydrophobic particles.

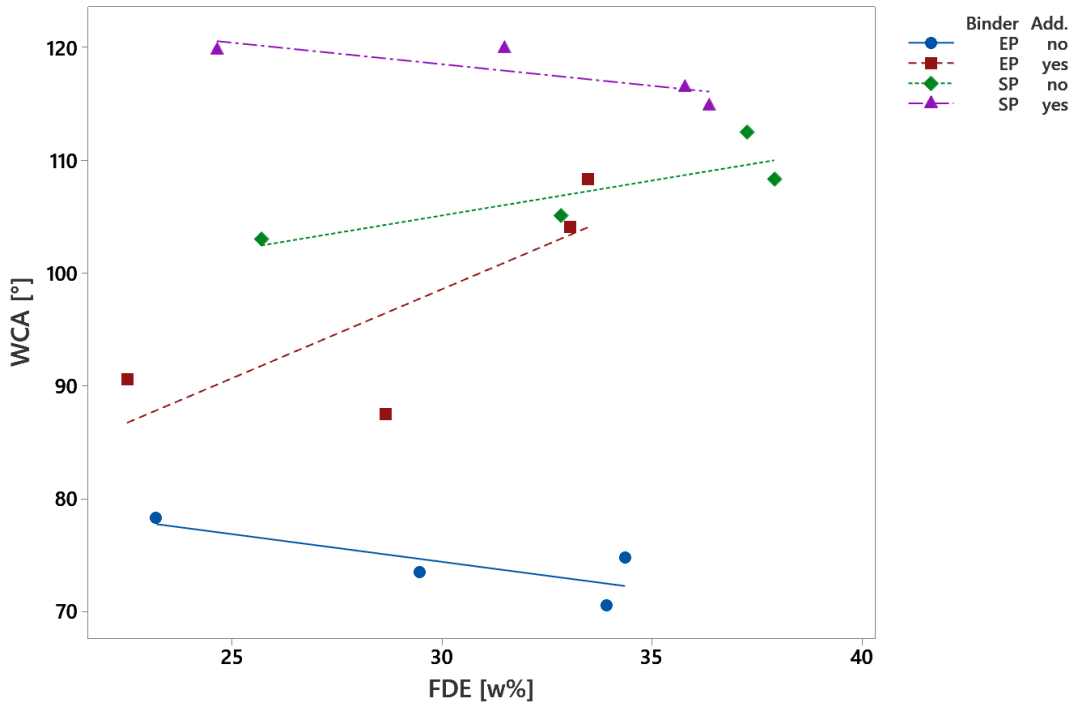

Figure 27: Fitted line plot of WCA vs. weight percentage of FDE for samples with FDE and aerosil at high Λ-values grouped by the presence of additive and the type of binder.

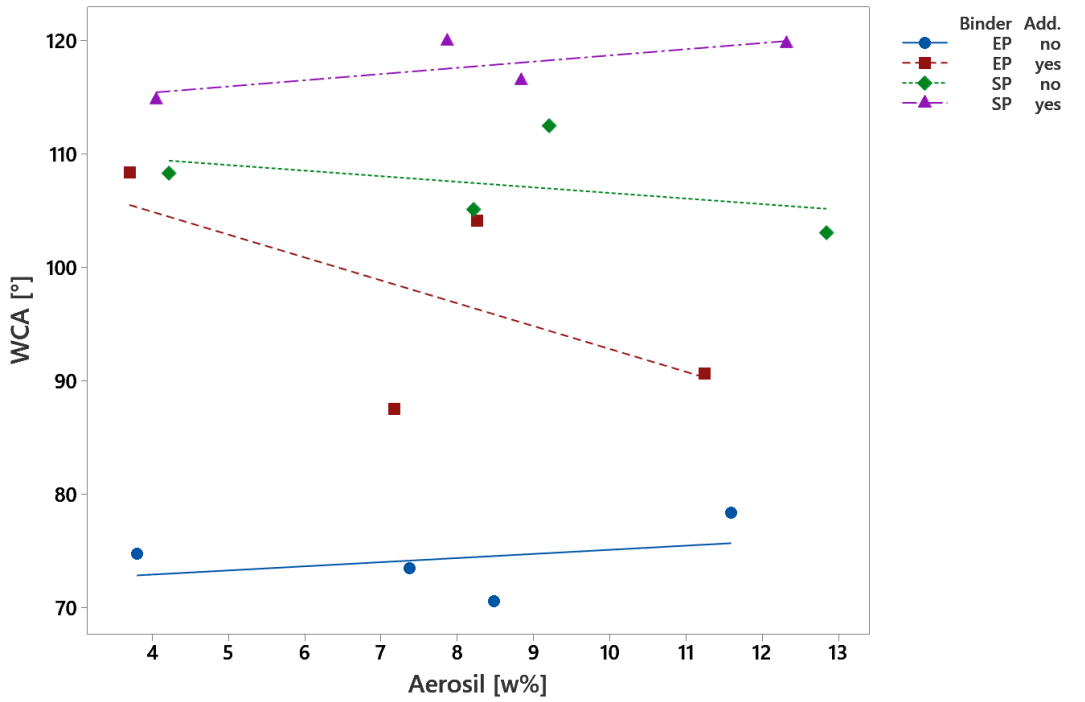

Figure 28: Fitted line plot of WCA vs. weight percentage of aerosil for samples with FDE and aerosil at high Λ-values grouped by the presence of additive and the type of binder.

In Table 21 the results from the regression analysis with RMS curvature as the response is presented. The R^2-value for the model is similar to other models in this study at 73.9%. In accordance with previous results, the increase in FDE increases the RMS curvature of

the samples. Unexpectedly, the type of binder used seems to affect the RMS curvature as well. The binders might be interacting differently with the added aerosil at high Λ-values. The positive T-value of the term in the model indicate that the Epoxy binder show higher RMS curvature values than Silikopon EF, while the results in Table 20 indicate that the WCA is higher for Silikopon EF than Epoxy. This means a higher RMS curvature with lower displays of hydrophobicity.

Table 21: The effect of binder, additive and amount of FDE and aerosil for high Λ-values on RMS curvature. The R^2-value for the model is 73.9%.

Term	**T-value**	**p-value**
Binder	2.16	0.0501
FDE	6.06	4.05×10^{-5}

Analysing the RMS curvature results further one might get a better understanding of the regression results. Figure 29 display fitted line plots for samples with a combination of aerosil and FDE and high Λ-values of RMS curvature vs. weight percentage of FDE. The values are grouped by the presence of the additive and the type of binder. The fitted lines do show a clear favour of higher RMS curvature for samples with Epoxy binder. The sample with the highest RMS curvature is the samples with Epoxy and no additive. These are also the samples that showed hydrophilic surfaces, as seen in Table 19 where the four samples all display WCA's less than 80°. Most likely, there is a wetting of the particles at the surface by the hydrophilic binder which then causes the surface roughness to increase the hydrophilicity of the surface instead of the hydrophobicity. This corresponds to the Wenzel model described in Section 2.3.

The differences in WCA and RMS curvature results might be due to different wetting of the particles based on the binder used. The Epoxy binder might be wetting the particles more which results in lower chemical hydrophobicity while there is still a high surface roughness. If Silikopon EF wets the particles at the surface less, this may also allow the aerosil particles to add nanoroughness to the surface, increasing the hydrophobicity. The samples with Silikopon EF and the additive are the only samples that do not show lower levels of hydrophobicity for lower weight percentages of FDE, meaning these samples show high levels of hydrophobicity adding aerosil and reducing FDE.

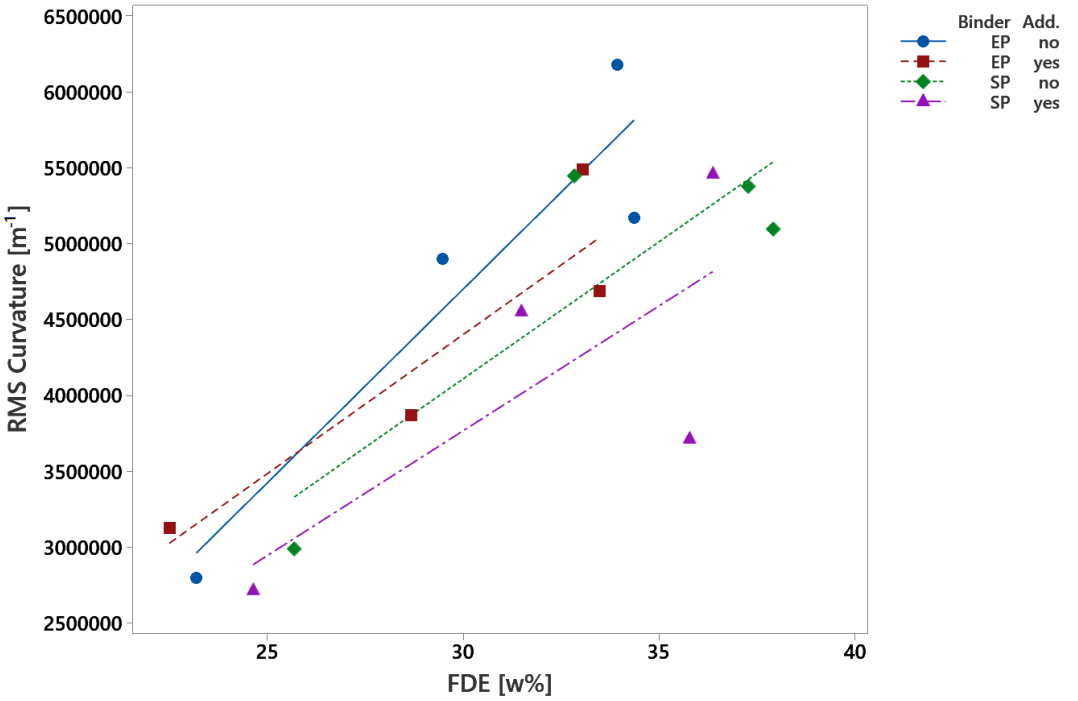

Figure 29: Fitted line plot of RMS curvature vs. weight percentage of FDE for samples with FDE and aerosil at high Λ-values grouped by the presence of additive and the type of binder.

Overall, the WCA of the samples used in this analysis were much lower than expected. By using both FDE and aerosil there would ideally be a hierarchical roughness with highly hydrophobic particles resulting in high WCA's. Instead, there was mostly no effect or, in some cases, a negative effect of combining the FDE and aerosil. Most likely due to less FDE being used to achieve the same Λ-values and the aerosil being completely wetted by the binder. For the samples with Epoxy and no additive the aerosil decreased the measured WCA of the samples. Thus, the combination of FDE and aerosil was not a success.

4.8 The effect of amount of additive, FDE and nanosilica particles in Silikopon EF binder

In order to possibly achieve a hierarchical roughness, samples were prepared with different ratios of FDE and nanosilica particles. The nanosilica particles are hydrophobic and of the size range 20 to 30 nm. The Sensofar microscope with the available microscopes cannot detect roughness smaller than approximately 0.7 microns, but its effect on the water contact angle was still valuable to explore. Statistical analyses with the amount of additive, Λ-values and the ratio between FDE and total amount of particles (FDE and nanosilica) as predictors and WCA and RMS curvature as responses were performed. An overview of all the predictors and responses used in the analysis before forward selection was performed is given in Table 22. Information about paint ingredients and results of individual samples are presented in Table 23.

Table 22: Overview of predictors and responses used in the regression models displayed in this section before forward selection was performed with the Silikopon EF binder.

Responses	**Predictors**
Contact angle	Additive, Λ, Ratio of FDE/total particles
RMS curvature	Additive, Λ, Ratio of FDE/total particles
RMS curvature	Additive, FDE, Nanosilica

Table 23: An overview of the samples and their results used in the statistical analysis of amount of additive, nanosilica (NS) and FDE in the Silikopon EF binder. The ratio refers to the weight of FDE over the weight of both FDE and nanosilica.

Sample	**TP** [w%]	**FDE** [w%]	**NS** [w%]	**Ratio**	**Λ**	**WCA** [°]	**h"** [$\mathbf{Mm^{-1}}$]
SP_FDE50_NSi50_TP2_02	2.0	4.7	4.7	50	0.20	98.0	0.0727
SP_FDE50_NSi50_TP2_04	2.0	9.1	9.1	50	0.40	95.3	0.0865
SP_FDE50_NSi50_TP2_06	2.0	13	13	50	0.60	97.3	2.10
SP_FDE50_NSi50_TP2_08	2.0	17	17	50	0.8	104	3.71
SP_FDE50_NSi50_TP2_10	2.0	20	20	50	1.0	90.6	2.04
SP_FDE50_NSi50_TP2_12	2.0	23	23	50	1.2	97.7	3.87
SP_FDE50_NSi50_TP4_02	4.0	4.6	4.6	50	0.20	95.3	0.0547
SP_FDE50_NSi50_TP4_04	4.0	8.9	8.9	50	0.40	94.4	0.308
SP_FDE50_NSi50_TP4_06	4.0	13	13	50	0.60	91.3	2.20
SP_FDE50_NSi50_TP4_08	4.0	16	16	50	0.80	122	4.25
SP_FDE50_NSi50_TP4_10	4.0	19	19	50	1.0	119	6.61
SP_FDE50_NSi50_TP4_12	4.0	22	22	50	1.2	121	5.81
SP_FDE25_NSi75_TP2_0	2.0	2.3	6.7	25	0.20	93.1	0.0495
SP_FDE25_NSi75_TP2_04	2.0	4.3	13	25	0.40	96.2	0.121
SP_FDE25_NSi75_TP2_06	2.0	6.2	19	25	0.60	92.0	1.85
SP_FDE25_NSi75_TP2_08	2.0	7.8	24	25	0.80	89.3	2.11
SP_FDE25_NSi75_TP2_10	2.0	8.5	30	25	1.0	111	4.32
SP_FDE25_NSi75_TP2_12	2.0	11	33	25	1.2	106	4.18
SP_FDE25_NSi75_TP4_02	4.0	2.2	6.6	25	0.20	93.5	0.0550
SP_FDE25_NSi75_TP4_04	4.0	4.2	13	25	0.40	92.9	0.127
SP_FDE25_NSi75_TP4_06	4.0	6.1	19	25	0.60	96.9	0.434
SP_FDE25_NSi75_TP4_08	4.0	7.7	23	25	0.80	106	2.72
SP_FDE25_NSi75_TP4_10	4.0	8.3	29	25	1.0	112	4.32
SP_FDE25_NSi75_TP4_12	4.0	11	32	25	1.2	115	5.65
SP_FDE75_NSi25_TP2_02	2.0	7.0	2.5	75	0.20	94.3	0.0931
SP_FDE75_NSi25_TP2_04	2.0	13	4.6	75	0.40	95.5	1.38
SP_FDE75_NSi25_TP2_06	2.0	19	6.5	75	0.60	89.7	1.76
SP_FDE75_NSi25_TP2_08	2.0	24	8.2	75	0.80	91.5	0.462
SP_FDE75_NSi25_TP2_10	2.0	31	9.5	75	1.0	118	4.78
SP_FDE75_NSi25_TP2_12	2.0	34	11	75	1.2	93.0	1.07
SP_FDE75_NSi25_TP4_02	4.0	6.6	2.4	75	0.20	94.8	0.0886
SP_FDE75_NSi25_TP4_04	4.0	13	4.5	75	0.40	95.9	0.298
SP_FDE75_NSi25_TP4_06	4.0	19	6.4	75	0.60	96.2	1.92
SP_FDE75_NSi25_TP4_08	4.0	23	8.0	75	0.80	95.9	1.48
SP_FDE75_NSi25_TP4_10	4.0	30	9.3	75	1.0	111	4.80
SP_FDE75_NSi25_TP4_12	4.0	22	11	75	1.2	108	4.48
SP_TP2_00	2.0	0.00	0.00	0.00	0.00	91.3	0.243
SP_TP4_00	4.0	0.00	0.00	0.00	0.00	96.3	0.125

As expected, the results of the model in Table 24 shows that the WCA increases with increasing Λ-values. Increasing the Λ-value results in more non-wetted hydrophobic particles. Consequently, the hydrophobicity of the particles and the roughness they form results in a higher WCA. The additive term has a positive T-value and small p-value which means that increasing the amounts of additive from 2 wt% to 4 wt% increases the hydrophobicity

of the paint. However, the model has an R^2-value of only 43.0% which is much lower than previous models. Figure 30 shows fitted line plots for WCA vs. Λ for samples with 4 wt% additive. The values are grouped by the ratio between the weight of FDE to total weight of both FDE and nanosilica. Increasing the fraction of FDE does not necessarily translate to an increase in WCA's. Instead, the highest hydrophobicity of these samples are gained with a 1:1 ratio between FDE and nanosilica particles. The regression analysis, therefore underperforms, as one of the predictors has an effect on the WCA, but is not included in the model due to its non-linear trend.

Table 24: The effect of the amount of additive, the Λ-value and ratio of FDE and nanosilica on the water contact angle. The R^2-value for the model is 43.0%.

Term	T-value	p-value
Additive	2.44	0.0199
Lambda	4.50	7.19×10^{-5}

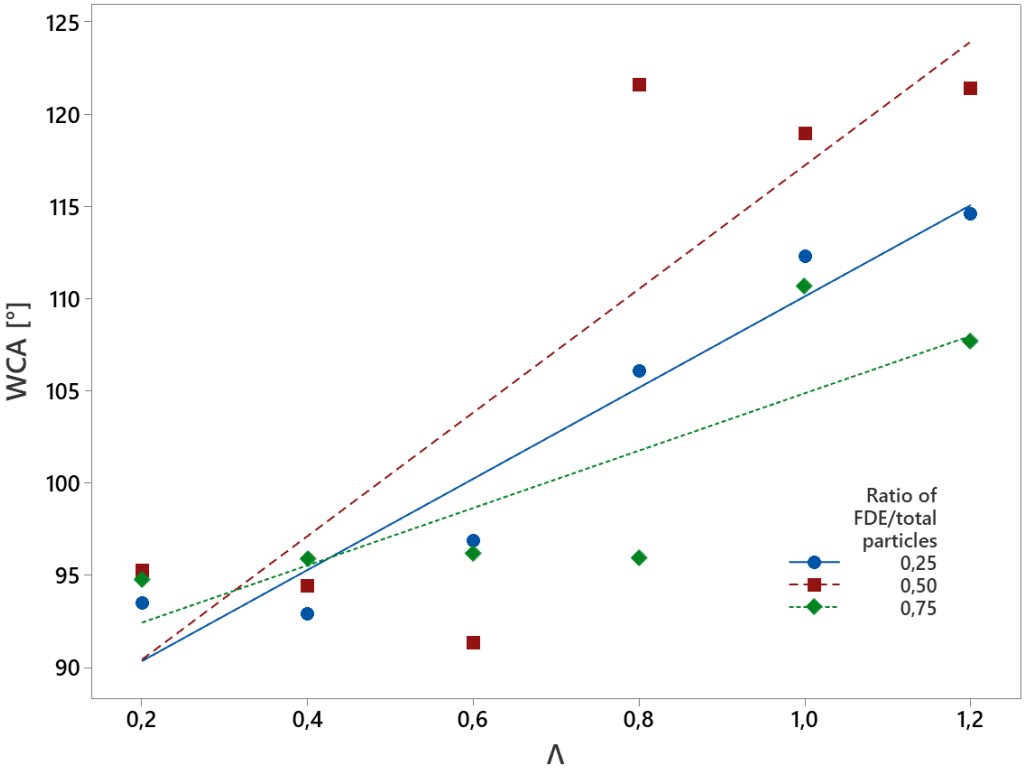

Figure 30: Fitted line plot of WCA vs. Λ grouped by the ratio of FDE/total particles. All samples contain 4 wt% of additive.

The model with the amount of additive, Λ-value and ratio of FDE and nanosilica as predictors and the RMS curvature as the response is presented in Table 25. As expected, the increase in the Λ-value increases the RMS curvature as this means an increase in the number of particles which will usually result in a rougher surface. The p-value of the Λ term is extremely small. The additive term has a p-value of 12.5% which is higher than the common level of significance 5%. The ratio term did not have a p-value of less than 25% and was therefore not included in the model. This was unexpected since the microscopy methods used would not be expected to capture the roughness contributed by the very

small nanosilica particles and thus a high ratio of FDE would be expected to increase the roughness observed.

Therefore, a model with the amounts of additive, FDE and nanosilica (not the ratio) as predictors and the RMS curvature as the response was performed, presented in Table 26. The additive term has a p-value of 9.11% which is higher than the level of significance of 5%. As expected, the FDE term has a positive T-value and a very small p-value. This is consistent with all the previous models in this study as increasing the amount of FDE particles directly increases the roughness of the surface. A surprising result was the extremely low p-value of the nanosilica term. This means that the RMS curvature increases when increasing the amount of nanosilica. The nanosilica consists of particles with a smaller size range than the microscope used in the study can detect. It might be expected that the particles agglomerate to form particles large enough to cause an increase in the roughness within the resolution range of the microscope, which is approximately 0.7 microns and larger.

Table 25: The effect of the amount of additive, the Λ-value and ratio of FDE and nanosilica on the RMS curvature. The R^2-value for the model is 69.9%.

Term	**T-value**	**p-value**
Additive	1.57	0.125
Lambda	8.87	1.78×10^{-10}

Table 26: The effect of the amount of additive, FDE and nanosilica on the RMS curvature. The R^2-value for the model is 70.5%.

Term	**T-value**	**p-value**
Additive	1.74	0.0911
FDE	5.11	1.24×10^{-5}
Nanosilica	6.78	8.63×10^{-8}

In order to further examine the effect of the ratio between FDE and total particles on the RMS curvature, fitted line plots of RMS curvature vs. Λ grouped by the ratio of FDE over total particles are displayed in Figure 31. As a mixture of a 1:1 ratio of FDE and nanosilica particles clearly shows the highest RMS curvature, which corresponds to this ratio also displaying the highest level of hydrophobicity.

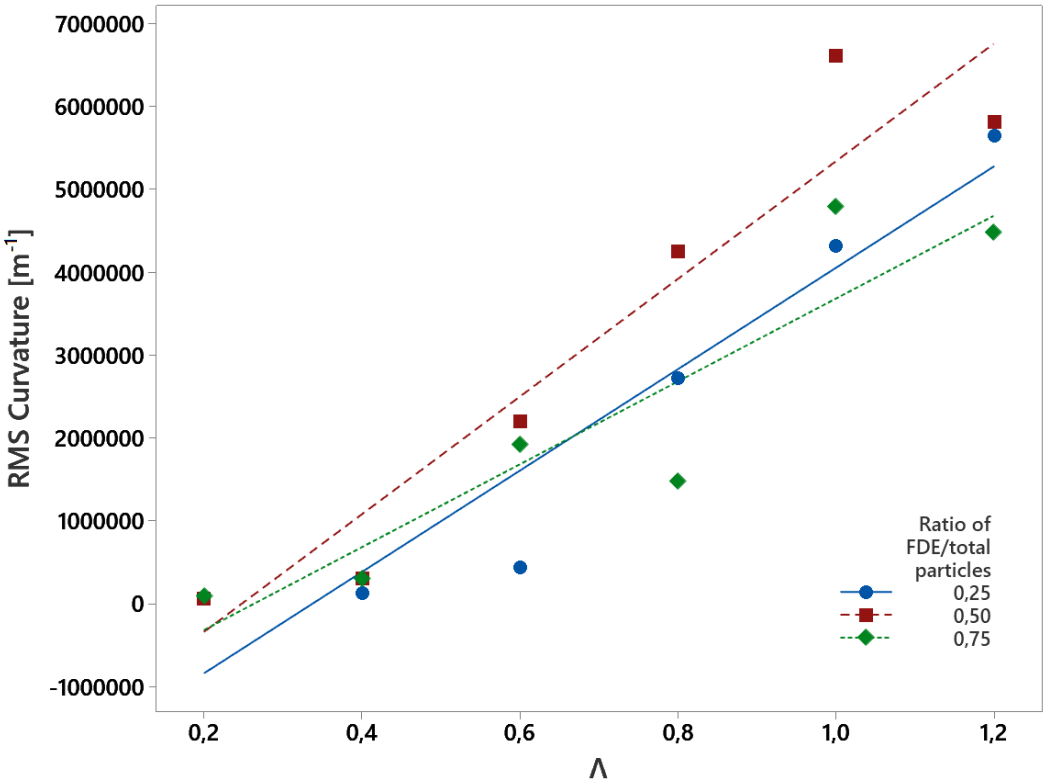

Figure 31: Fitted line plot of RMS curvature vs. Λ grouped by the ratio of FDE/total particles. All samples contain 4 wt% of additive.

4.9 The effect of additive and amount of FDE with a new binder, Dowsil

One of the reasons why it is difficult to achieve a very high hydrophobicity with the paint ingredients available might be due to a lack of a more hydrophobic binder. Both the Epoxy binder and the Silikopon EF binder without any added particles or additives have water contact angles of slightly below 90°. They show a slightly hydrophilic behaviour, which is not ideal for the purpose of creating a superhydrophobic coating. Therefore, a different binder, Dowsil, was used to try to increase the hydrophobicity even further. Table 27 shows the responses and predictors used in the regression analyses before forward selection was performed. An overview of paint ingredients of the samples used and the results are presented in Table 28.

Table 27: Overview of predictors and responses used in the regression models displayed in this section before forward selection was performed with Dowsil binder.

Responses	**Predictors**
Contact angle	Additive, FDE
RMS curvature	Additive, FDE

Table 28: An overview of the samples and their results used in the statistical analysis of additive and amount of FDE with the Dowsil binder.

Sample	**TP [w%]**	**FDE [w%]**	Λ	**WCA [°]**	**h" [Mm^{-1}]**
DO_FDE_00	0.00	0.00	0.00	93.4	0.0199
DO_FDE_04	0.00	24	0.40	89.1	0.804
DO_FDE_06	0.00	38	0.60	119	5.33
DO_FDE_08	0.00	54	0.8	113	5.46
DO_FDE_10	0.00	73	1.0	118	5.65
DO_FDE_12	0.00	94	1.2	114	5.90
DO_FDE_TP_00	4.0	0.00	0.00	92.3	0.126
DO_FDE_TP_04	4.0	22	0.40	93.9	1.45
DO_FDE_TP_06	4.0	36	0.60	122	6.45
DO_FDE_TP_08	4.0	51	0.80	119	6.65
DO_FDE_TP_10	4.0	68	1.0	119	6.83
DO_FDE_TP_12	4.0	87	1.2	131	6.62

In Table 29 the results from a regression analysis with WCA as the response is presented. The presence of the additive does not seem to affect the WCA significantly and is therefore not a part of the regression model. This might be due to the binder already displaying hydrophobic behaviours. The binder without any added additives or particles has a WCA of 93.4°, as seen in Table 28. However, as expected, the FDE has a positive effect on the WCA. The model has a lower R^2-value than many others in this study at only 60.4%.

Table 29: The effect of additive and amount of FDE on the water contact angle. The R^2-value for the model is 65.0%.

Term	**T-value**	**p-value**
FDE	4.31	1.52×10^{-3}

In Table 30 the results with RMS curvature as the response are displayed. As expected, the RMS curvature increases with the weight percentage of FDE. There might be an increase in RMS curvature with the presence of the additive, as the additive term has a p-value of 0.229, but there is not enough difference relative to the variance between the two to draw a conclusion.

Table 30: The effect of additive and amount of FDE on RMS curvature. The R^2-value for the model is 81.1%.

Term	**T-value**	**p-value**
FDE	6.12	1.74×10^{-4}
Additive	1.29	0.229

Due to the lower than expected R^2-value of the model presented in Table 29, a further examination of the paint sample composition and the WCA and RMS curvature of the samples is necessary. The sample results are displayed in fitted line plots of WCA vs. weight percentages of FDE grouped by the presence of the additive (Figure 32) and RMS curvature vs. weight percentages of FDE also grouped by the presence of the additive is

shown in Figure 33. As expected, low amounts of FDE show low levels of hydrophobicity and roughness. However, there is a drastic change in the level of hydrophobicity and roughness for weight percentages of FDE corresponding to Λ-values of 0.60 and higher. This is a change one would expect to happen at around $\Lambda = 1$ since the coating reaches the critical pigment volume concentration. Calculating the Λ-value is a highly uncertain process as wetting properties are measured for a reference binder and then generalised.

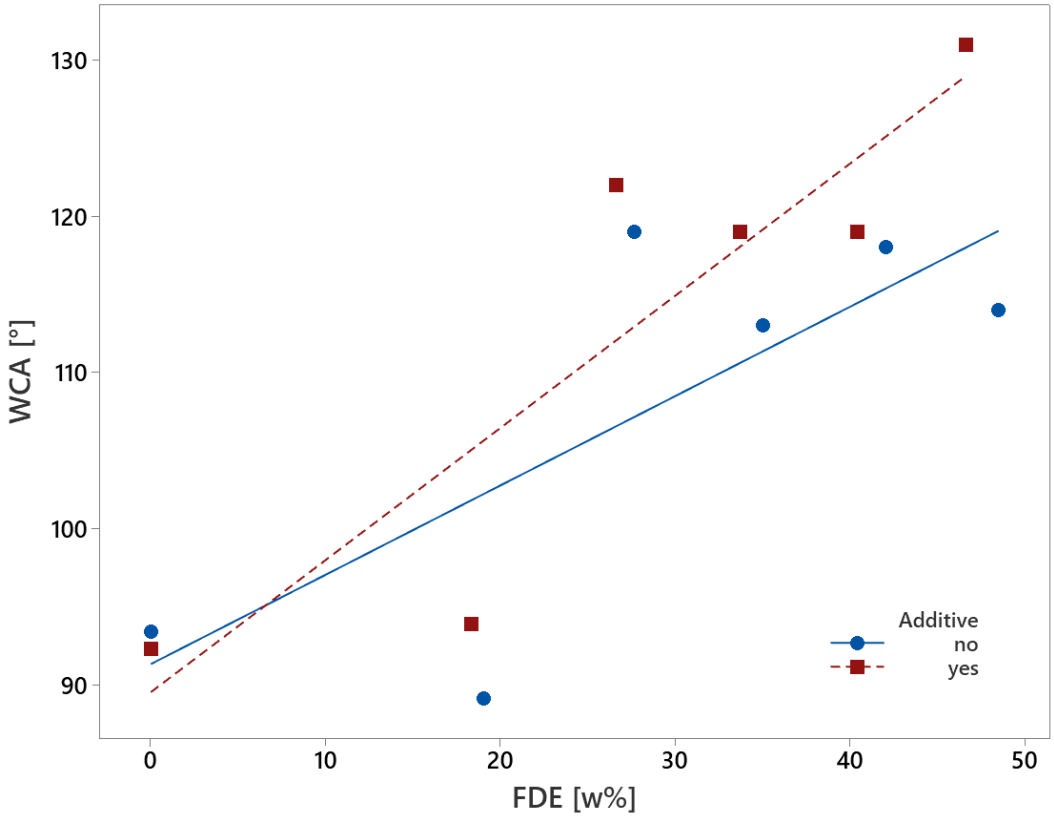

Figure 32: Fitted line plot of WCA vs. weight percentage of FDE for the samples with the Dowsil binder grouped by the presence of the additive.

The correlation between the amount of FDE and WCA, therefore, seems to plateau after reaching $\Lambda = 0.6$, which is most likely the reason why R^2-value of the model is lower than expected. There is however an exception to the plateau which is sample DO_FDE_TP_12. This sample has a Λ-value of 1.2 and with the presence of the additive it reaches a WCA of 131°, which is higher than any other sample in this study. However, the RMS curvature values of the samples with higher levels of FDE are similar, as seen in Figure 33. It has to be mentioned that this was one of the samples that were thinned before draw down. This might have caused the binder to either wet the particles at the surface with a thinner layer or not wetting the particles at all, exposing them fully at the surface. This could then increase the chemical hydrophobicity of the surface or increase a lower scale of roughness which the methods used in this study is not able to detect. Apart from this single sample, the Dowsil binder generally does not display any better results than the Silikopon EF or the Epoxy binder.

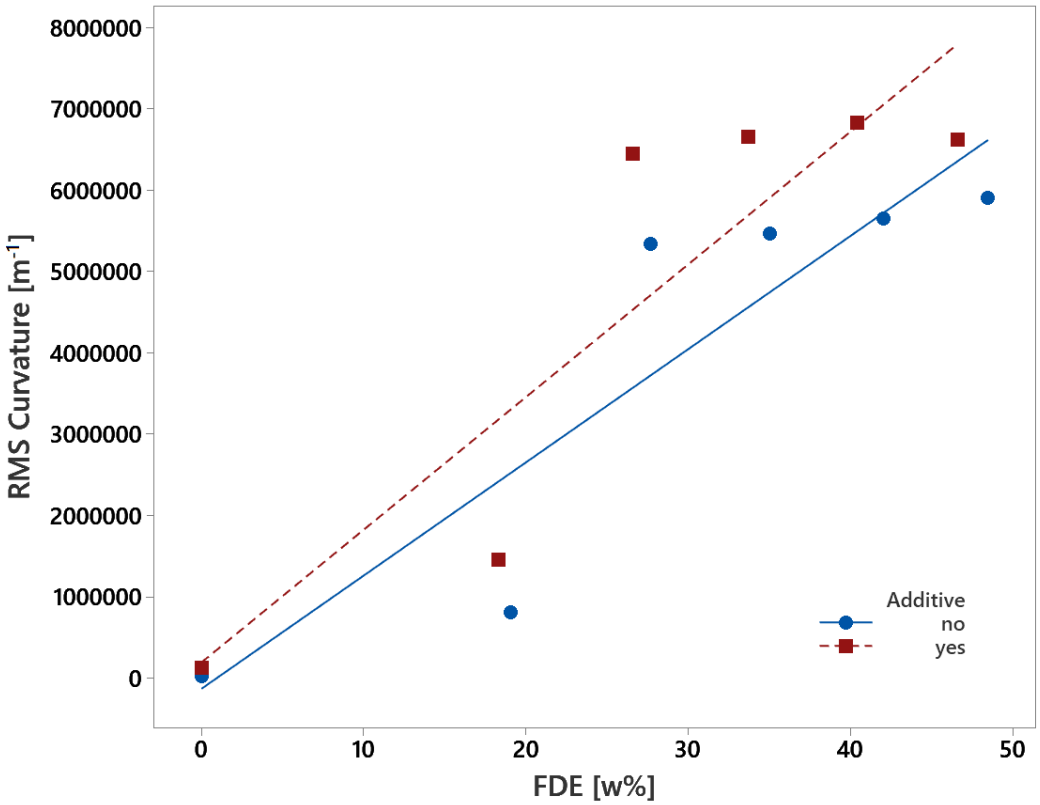

Figure 33: Fitted line plot of RMS curvature vs. weight percentage of FDE for the samples with the Dowsil binder grouped by the presence of the additive.

4.10 Summary of results from statistical analysis

Statistical analysis has been performed on the samples in order to map the effect of roughness values, type of binder, the presence of the additive, amounts of FDE, aerosil and nanosilica. An overview of all the regression models performed with predictors, responses before forward selection and responses after forward selection is presented in Table 31.

Table 31: Overview of results from all regression models, showing both the responses before forward selection (FS) and after FS. Predictors of samples with binders Silikopon EF and Dowsil are denoted SP and D respectively.

Predictor	**Responses before FS**	**Responses after FS**
WCA	Binder, Additive, h″	Binder, Additive, h″
WCA	Binder, Additive, h′	Binder, Additive, h′
WCA	Binder, Additive, h	Binder, h
h″	h′	h′
WCA	Functionalisation, h″	Functionalisation, h″
h″	DE, Functionalisation	DE, Functionalisation
WCA	Binder, Additive, FDE	Binder, Additive, FDE, Binder×FDE
h″	Binder, Additive, FDE	Additive, FDE
WCA	Binder, Additive, FDE, Aerosil	Binder, Additive
h″	Binder, Additive, FDE, Aerosil	Binder, FDE
WCA (SP)	Additive, Λ, Ratio: FDE/tot. particles	Additive, Λ
h″ (SP)	Additive, Λ, Ratio: FDE/tot. particles	Additive, Λ
h″ (SP)	Additive, FDE, Nanosilica	Additive, FDE, Nanosilica
WCA (D)	Additive, FDE	FDE
h″ (D)	Additive, FDE	FDE

The regression models favour the use of Silikopon EF binder, the presence of the additive and high amounts of FDE. When examining fitted line plots, the effect of binder and additive diminishes for high Λ-values, meaning that the surface roughness, and perhaps the chemical hydrophobicity, of adding large amounts of particles dominate the apparent hydrophobicity of the binder. The particles with the best performance was FDE or a mixture of a 1:1 ratio of FDE and nanosilica particles.

4.11 Superhydrophobic surface with double-sided tape and aerosil

The paint samples created for the regression analysis did not show contact angles higher than around 130°. In order to create a surface that actually showed superhydrophobic tendencies, with a contact angle of around 150° or more, a sample with double-sided tape layered with aerosil particles was prepared. Aerosil is a highly hydrophobic particle but has not showed promising results when added to a binder system. In a binder system the particles might be wetted by the binder, lowering the chemical hydrophobicity of the top layer and levelling the surface, decreasing the roughness. However, when aerosil particles are layered on top of tape all the particles will be exposed and there will be a random distribution of particles which will create roughness.

The measured contact angle of the tape layered with aerosil exceeded 140° though it was difficult to measure due to the surface being very hydrophobic and having a low roll-off angle making the water droplets bounce off the surface. In order to measure the relative roughness of adding aerosil to the tape, roughness measurements were performed also on a surface with just tape and no aerosil.

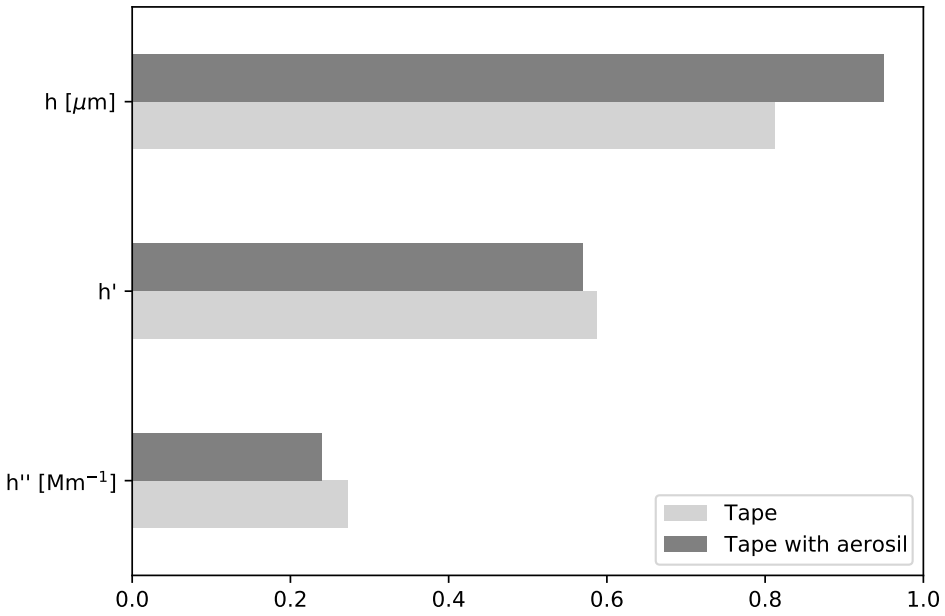

Figure 34: Bar chart displaying the difference in RMS roughness (h), slope (h′) and curvature (h″) for the sample with tape and the sample with tape and a layer of aerosil.

In Figure 34 the difference in roughness values is displayed in a bar chart for the sample with tape and the sample with tape and a layer of aerosil. Due to a level of uncertainty associated with using the PSD curves to calculate the roughness values, observing the differences in Figure 34 one could assume there is no significant difference in roughness observed on the scale measured. However, due to the large difference in hydrophobicity, it can be expected that the surface roughness is different on a sub-micrometre scale. The chemical nature of the surface, with no roughness, can in theory only increase the contact angle up to around 120° which is significantly lower than what was measured for the tape and aerosil sample[31]. Figure 35 shows a SEM image of aerosil. The particle size is in the nanometre range with some agglomeration in the micrometre range. The microscopic techniques used to measure the surface do not have high enough resolution to detect the level of roughness one might expect the aerosil to create. This very small-scaled roughness might be participating in the increased hydrophobicity.

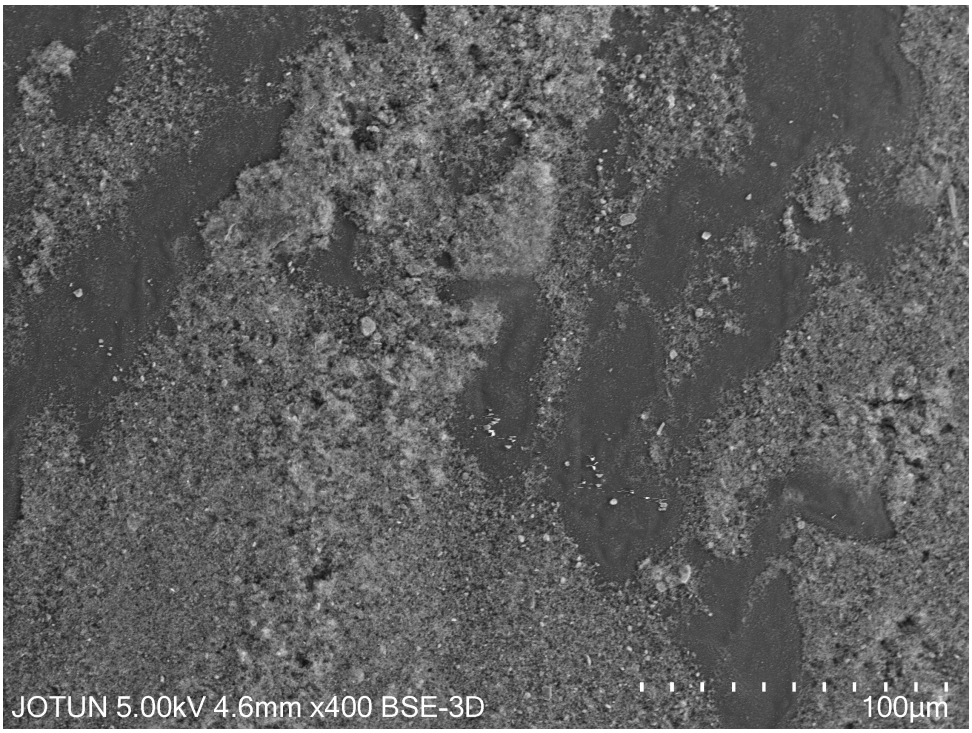

Figure 35: SEM image of aerosil.

One can observe some difference in roughness in the PSD functions of the two samples. When zooming in on the spatial frequency range of 1 to 8 $Mm^{-}1$ of the functions used to calculate RMS curvature by integration, as demonstrated in Figure 36, one can see a higher intensity for the sample tape with aerosil. This range of spatial frequencies corresponds to wavelengths down to approximately 0.7 microns. Aerosil particles are smaller than this, but agglomerations of particles can be expected due to electrostatic attraction and larger particle sizes are therefore possible. The increase in roughness for this size range might be the cause of the higher water contact angle, but most likely it is due to an even smaller-scaled roughness or a combination of these two. In order to confirm this, a microscopy technique with a higher resolution, such as an atomic force microscope, has to be used.

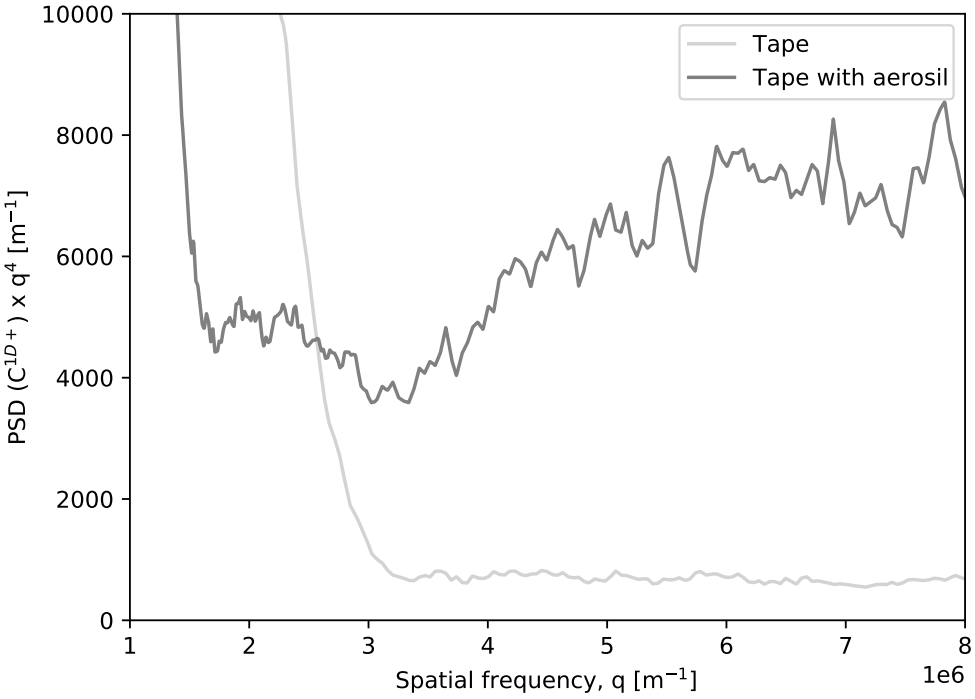

Figure 36: PSD functions of sample with tape and sample with tape layered with aerosil, multiplied by the spatial frequency 4 times in order to increase the weighting of higher spatial frequencies. They are the functions integrated in order to calculate the RMS curvature. The y-range is set to 0 to 10000 m^{-1} and x-range is between 1 to 8 Mm^{-1}.

4.12 Proposed wetting theory

As regression models and examinations of fitted line plots highlighted, the interactions between binders, particles and additives are unpredictable. In order to perhaps explain some of the unexpected results, a wetting theory is proposed.

The proposed wetting theory is displayed as a schematic drawing in Figure 37. In a) the particle is not wetted by the binder, thus being fully exposed at the surface. In b) the particle is wetted by the binder, but by a thin layer and therefore the sub-micro- and nanoroughness of the particle is still represented at the surface. Finally, in c) the particle is wetted by the binder by a thick layer, completely covering the particle and removing the roughness of the particle from the surface. This thick layer might also slightly increase the microroughness of the surface, represented in the RMS curvature and slope in this study, which cannot be distinguished from sub-microroughness due to the missing high-resolution analysis. The reasoning behind why these different wetting states might occur is assumed to be due to mainly three things. First, the amount of particles added to the paint formulation. Higher Λ-values would most likely result in a higher likelihood of particles being in state a) or b). Second, the binder and particles interact with each other differently based on attractions. One could for example expect that a hydrophilic binder might be less inclined to wet a more hydrophobic particle. Third, the viscosity of the binder system might affect how the particles are wetted and especially affect the thickness of the layer of the binder.

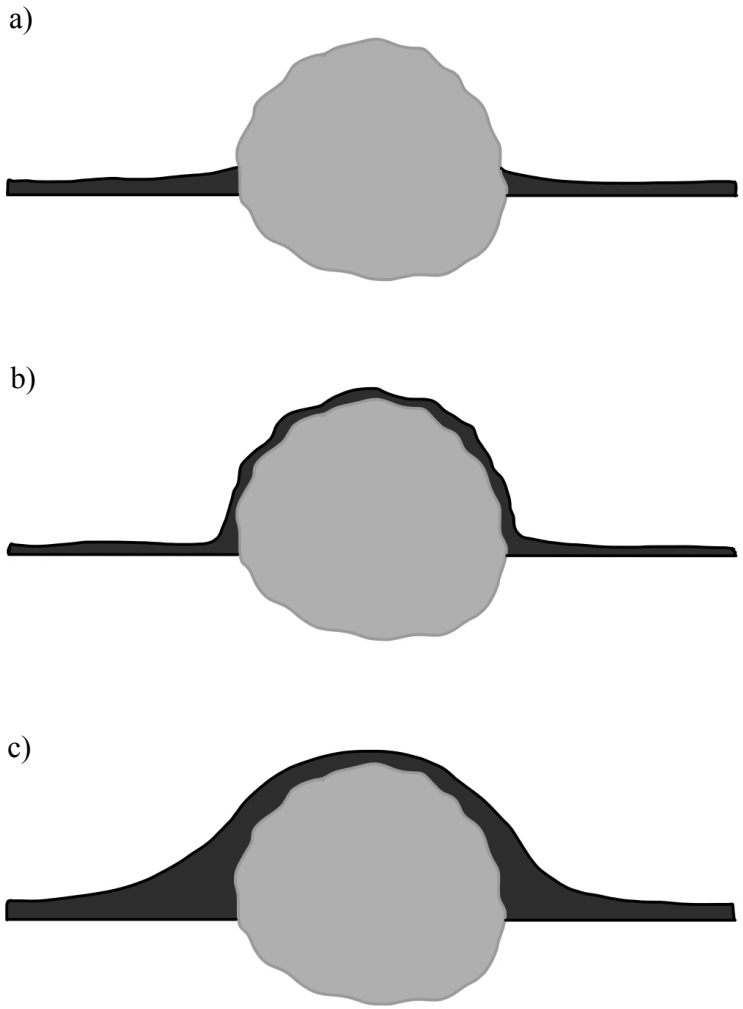

Figure 37: Schematic drawing of proposed wetting theory. a) Particle not wetted by binder and therefore exposed at the surface. b) Particle wetted by a thin layer of binder, some roughness from particle surface remains. c) Particle is wetted by the binder with a thick layer, nanoroughness from particle surface diminished, but microroughness might be slightly increased.

A more thorough examination of the three wetting states have to be performed in order to confirm this proposed theory, but some results in previous sections do give some support. Analysis of the effect of functionalising DE showed that samples with FDE had higher WCA's, but had a tendency to display lower values of RMS curvature. Therefore, in order for samples with FDE to have higher WCA's, the surface of the samples need either to be more chemically hydrophobic or show a higher level of roughness in the sub-micro to nanometre regime, not detected by the microscopy methods in this study. There is no significant difference in viscosity between samples with NFDE and FDE so the way in which the binder interacts with the particle is most likely what is affecting the wetting. Additionally, SEM photos showed differences in smaller-scaled roughness on individual DE particles. The FDE particle seemed to be less rounded. Further work is needed to see if samples with FDE and NFDE follow the non-wetting described in Figure 37 a) and therefore have exposed particles affecting the chemical hydrophobicity of the surface, thus samples with FDE showing higher levels of hydrophobicity. The samples with FDE could

be covered in a thinner layer of binder, according to wetting state b), and NFDE covered in a thicker layer, according to wetting state c), and therefore the nanoroughness of the DE particles increase the hydrophobicity. Samples with NFDE showed a tendency for higher RMS curvature values. This can be explained by a layer of binder shown in Figure 37 b) and c).

In Section 4.6, samples with Silikopon EF binder and no additive displayed comparatively high WCA's while showing a tendency for lower values of RMS curvature than other samples with the same weight percentages of FDE. This was not the case for samples with Epoxy binder and no additive, as those samples showed a tendency for both lower WCA's and lower RMS curvature values. One reason for this might be that Silikopon EF without an additive wet the FDE less due to the binder being less hydrophobic, thus not being attracted to the hydrophobic FDE particles. This could expose the FDE particle at the surface, allowing its chemical hydrophobicity to increase the WCA's of the samples. As the particle is not covered by a layer of the binder, the micro-scale roughness might be slightly lower, resulting in lower values of RMS curvature. For samples with Epoxy binder, the results seem to be less complicated and the reason for the lower WCA's displayed by samples with no additive is a result of their lower RMS curvature values. It has already been established in Section 4.3 that the additive does add some level of roughness to the samples.

For the samples with high Λ-values and a combination of FDE and aerosil particles there is again some unexpected results of WCA's and RMS curvature values. Generally, the Silikopon EF samples showed the highest WCA's, but the Epoxy samples showed higher RMS curvature values. The Silikopon EF binder might wet the FDE and aerosil particles less, allowing either their nanoroughness or their chemical hydrophobicity to be exposed at the surface, resulting in higher WCA's.

The importance of paint viscosity is highlighted by a sample with Dowsil binder, an additive and FDE with a Λ-value of 1.2 in Section 4.9 which displayed the highest WCA in this study at 131°. Due to its high Λ-value, the draw down was challenging and it was therefore thinned with Xylene. A draw down was made with the not-thinned version of the sample which displayed a WCA of 114°, which was lower than samples with the same components and lower Λ-values. These differences in WCA's might be due to the thickness of the binder layer wetting the FDE particles at the surface in the presence or not presence of more solvent. The thinned sample might have a thinner layer of binder at the surface, thus allowing the nanoroughness of the FDE particles to define the surface, whereas the binder in the not-thinned sample might cover the particles with a thicker layer. As paint formulation with more solvent needs more time to harden in addition to having lower viscosity, the binder might spread and level out more, allowing for the particles' nanoroughness to define the surface roughness more. Paint formulations with less solvent harden faster, so the particles might spread out less which results in higher large-scale roughness, but less nanoroughness.

This section has highlighted the possible ways in which the binder might wet the surface particles, but further examination is needed in order to confirm the proposed wetting theory.

5 Conclusion and further work

Statistical analyses have been performed in order to examine various paint ingredients' effect on hydrophobicity and surface roughness values calculated from PSD functions of topography measurements. The roughness values RMS roughness, slope and curvature from the PSD functions were studied. A regression analysis showed clear correlation between RMS curvature and WCA's. Correlation between RMS slope and WCA's were also discovered, but there was also a high level of correlation between RMS slope and roughness. This highlighted a limitation of the model as the microscopy methods used did not possess a high enough resolution to capture sub-microroughness and nanoroughness. Ideally, the model would include roughness values which differentiated between microroughness and nanoroughness in order to examine the effect of hierarchical roughness on the hydrophobicity.

Regression analyses of paint ingredients favoured Silikopon EF binder, the presence of an additive and high weight percentages of FDE. Though for high weight percentages of FDE, a more thorough examination by fitted line plots showed less dependence on binder and the presence of the additive in order to achieve high WCA's. A more hydrophobic binder, such as the Dowsil, did not show more promising results for high weight percentages of FDE compared to the two other binders used.

Due to unexpected variations in RMS curvature values and WCA's, a wetting theory was proposed. The wetting theory differentiates between the degree of wetting by the binder of the particles at the surface. Three types of wetting were proposed: non-wetting, wetting by a thin layer of the binder and wetting by a thick layer of the binder. This model was proposed in an attempt to explain the variations in RMS curvature and resulting WCA's.

Further work would involve a more thorough exploration of the proposed wetting model. This could involve using hydrophilic binders with hydrophobic particles, at high Λ-values, so the binder might be less inclined to wet the particles, exposing them at the surface. Using a more hydrophobic binder with hydrophilic particles could also be of interest. Additionally, microscopy methods with higher resolutions should be used in order to capture a smaller scale of roughness. This could allow the model to differentiate between microroughness and nanoroughness which are, according to literature, both needed in order to create a stable superhydrophobic surface. This could also allow for observations to possibly confirm the different types of wetting proposed in the wetting theory.

Bibliography

[1] *What is climate change?* URL: https://www.un.org/en/climatechange/what-is-climate-change..

[2] Sukhjit Singh and Vivian Rambarath-Parasram. 'Considerations for the Latin American and Caribbean region in light of the global move towards low carbon shipping'. In: *Best Practices in Manufacturing Processes*. Springer, 2019, pp. 53–73.

[3] Zheng Wan et al. 'Decarbonizing the international shipping industry: Solutions and policy recommendations'. In: *Marine pollution bulletin* 126 (2018), pp. 428–435.

[4] H Lackenby. 'The thirty-fourth Thomas Lowe gray lecture: resistance of ships, with special reference to skin friction and hull surface condition'. In: *Proceedings of the Institution of Mechanical Engineers* 176.1 (1962), pp. 981–1014.

[5] SHUJI Mizokami et al. 'Experimental study of air lubrication method and verification of effects on actual hull by means of sea trial'. In: *Mitsubishi Heavy Industries Technical Review* 47.3 (2010), pp. 41–47.

[6] Nanlin Yu et al. 'Facile preparation of durable superhydrophobic coating with self-cleaning property'. In: *Surface and Coatings Technology* 347 (2018), pp. 199–208.

[7] Tommaso Baldacchini et al. 'Superhydrophobic surfaces prepared by microstructuring of silicon using a femtosecond laser'. In: *Langmuir* 22.11 (2006), pp. 4917–4919.

[8] Seung Goo Lee et al. 'Switchable transparency and wetting of elastomeric smart windows'. In: *Advanced materials* 22.44 (2010), pp. 5013–5017.

[9] H.Y. Erbil. 'Surface Chemistry of Solid and Liquid Interfaces'. In: Wiley, 2006. Chap. 1 - Introduction to Surfaces and Interfaces. ISBN: 9781405119689.

[10] H.Y. Erbil. 'Surface Chemistry of Solid and Liquid Interfaces'. In: Wiley, 2006. Chap. 3 - Thermodynamics of Interfaces. ISBN: 9781405119689.

[11] DP Subedi. 'Contact angle measurement for the surface characterization of solids'. In: *Himalayan Physics* 2 (2011), pp. 1–4.

[12] J Song and OJ Rojas. *Approaching super-hydrophobicity from cellulosic materials: A 411 Review, Pap. Chem. 28 (2013) 216–238. doi: 10.3183*. Tech. rep. NPPRJ-2013-28-02-p216-238. 412.

[13] Alvaro Della-Bona. 'Characterizing ceramics and the interfacial adhesion to resin: II-the relationship of surface treatment, bond strength, interfacial toughness and fractography'. In: *Journal of Applied Oral Science* 13 (2005), pp. 101–109.

[14] CG Jothi Prakash and R Prasanth. 'Approaches to design a surface with tunable wettability: a review on surface properties'. In: *Journal of Materials Science* 56.1 (2021), pp. 108–135.

[15] Thomas Young. 'III. An essay on the cohesion of fluids'. In: *Philosophical transactions of the royal society of London* 95 (1805), pp. 65–87.

[16] Lasse Makkonen. 'Young's equation revisited'. In: *Journal of Physics: Condensed Matter* 28.13 (2016), p. 135001.

[17] Robert N Wenzel. 'Resistance of solid surfaces to wetting by water'. In: *Industrial & Engineering Chemistry* 28.8 (1936), pp. 988–994.

[18] Robert N Wenzel. 'Surface roughness and contact angle.' In: *The Journal of Physical Chemistry* 53.9 (1949), pp. 1466–1467.

[19] KG Grigorov et al. 'Optical and morphological properties of N-doped TiO2 thin films'. In: *Surface Science* 605.7-8 (2011), pp. 775–782.

[20] Michael Nosonovsky and Bharat Bhushan. 'Roughness optimization for biomimetic superhydrophobic surfaces'. In: *Microsystem Technologies* 11.7 (2005), pp. 535–549.

[21] ABD Cassie and S Baxter. 'Wettability of porous surfaces'. In: *Transactions of the Faraday society* 40 (1944), pp. 546–551.

[22] David E Packham. 'Surface energy, surface topography and adhesion'. In: *International journal of adhesion and adhesives* 23.6 (2003), pp. 437–448.

[23] Barbara Cortese et al. 'Superhydrophobicity due to the hierarchical scale roughness of PDMS surfaces'. In: *Langmuir* 24.6 (2008), pp. 2712–2718.

[24] C Yang, U Tartaglino and BNJ Persson. 'Influence of surface roughness on superhydrophobicity'. In: *Physical review letters* 97.11 (2006), p. 116103.

[25] Michael K Shepard, Robert A Brackett and Raymond E Arvidson. 'Self-affine (fractal) topography: Surface parameterization and radar scattering'. In: *Journal of Geophysical Research: Planets* 100.E6 (1995), pp. 11709–11718.

[26] Tevis DB Jacobs, Till Junge and Lars Pastewka. 'Quantitative characterization of surface topography using spectral analysis'. In: *Surface Topography: Metrology and Properties* 5.1 (2017), p. 013001.

[27] BNJ Persson. 'On the fractal dimension of rough surfaces'. In: *Tribology Letters* 54.1 (2014), pp. 99–106.

[28] Satoshi Shibuichi et al. 'Super water-repellent surfaces resulting from fractal structure'. In: *The Journal of Physical Chemistry* 100.50 (1996), pp. 19512–19517.

[29] Michael Nosonovsky and Bharat Bhushan. 'Hierarchical roughness optimization for biomimetic superhydrophobic surfaces'. In: *Ultramicroscopy* 107.10-11 (2007), pp. 969–979.

[30] Md Syam Hasan and Michael Nosonovsky. 'Lotus effect and friction: Does nonsticky mean slippery?' In: *Biomimetics* 5.2 (2020), p. 28.

[31] Michael S Bell et al. 'Effects of hierarchical surface roughness on droplet contact angle'. In: *Langmuir* 31.24 (2015), pp. 6752–6762.

[32] Nosonovsky Michael and Bharat Bhushan. 'Hierarchical roughness makes superhydrophobic states stable'. In: *Microelectronic engineering* 84.3 (2007), pp. 382–386.

[33] Weihua Li and A Amirfazli. 'Hierarchical structures for natural superhydrophobic surfaces'. In: *Soft Matter* 4.3 (2008), pp. 462–466.

[34] Bharat Bhushan and Yong Chae Jung. 'Natural and biomimetic artificial surfaces for superhydrophobicity, self-cleaning, low adhesion, and drag reduction'. In: *Progress in Materials Science* 56.1 (2011), pp. 1–108.

[35] John T Simpson, Scott R Hunter and Tolga Aytug. 'Superhydrophobic materials and coatings: a review'. In: *Reports on Progress in Physics* 78.8 (2015), p. 086501.

[36] TR Thomas. 'Characterization of surface roughness'. In: *Precision Engineering* 3.2 (1981), pp. 97–104.

[37] Khalid A Alshibli and Mustafa I Alsaleh. 'Characterizing surface roughness and shape of sands using digital microscopy'. In: *Journal of computing in civil engineering* 18.1 (2004), pp. 36–45.

[38] J.C. Stover and Society of Photo-optical Instrumentation Engineers. *Optical Scattering: Measurement and Analysis*. Press Monographs. SPIE Optical Engineering Press, 1995. ISBN: 9780819419347.

[39] NO Myers. 'Characterization of surface roughness'. In: *Wear* 5.3 (1962), pp. 182–189.

[40] RE Lobnig et al. 'Development of a new experimental method to determine critical pigment–volume–concentrations using impedance spectroscopy'. In: *Progress in organic coatings* 55.4 (2006), pp. 363–374.

[41] Nuno M Oliveira, Rui L Reis and Joao F Mano. 'Superhydrophobic surfaces engineered using diatomaceous earth'. In: *ACS applied materials & interfaces* 5.10 (2013), pp. 4202–4208.

[42] Angela Duparre et al. 'Surface characterization techniques for determining the root-mean-square roughness and power spectral densities of optical components'. In: *Applied optics* 41.1 (2002), pp. 154–171.

[43] Helmut H Toebben et al. 'Use of power spectral density (PSD) to specify optical surfaces'. In: *Specification, Production, and Testing of Optical Components and Systems*. Vol. 2775. International Society for Optics and Photonics. 1996, pp. 240–250.

[44] Abhijeet Gujrati et al. 'Combining TEM, AFM, and profilometry for quantitative topography characterization across all scales'. In: *ACS applied materials & interfaces* 10.34 (2018), pp. 29169–29178.

[45] KM Muraleedhara Prabhu. *Window functions and their applications in signal processing*. Taylor & Francis, 2014.

[46] Ronald E Walpole et al. *Probability and statistics for engineers and scientists*. Vol. 5. Macmillan New York, 1993.

[47] PLG Jardim et al. 'Determination of the Wenzel roughness parameter by the power spectral density of functional alumina surfaces'. In: *Thin Solid Films* 606 (2016), pp. 57–62.

Appendix

A Overview of samples used in Section 4.4

Table 32: An overview of the samples used in analysis of the effect of different roughness values on the WCA.

Sample	**TP** [w%]	**FDE** [w%]	**Aerosil** [w%]	Λ
SP_00	0.00	0.00	0.00	0.00
SP_FDE_04	0.00	21	0.00	0.40
SP_FDE_06	0.00	30	0.00	0.64
SP_FDE_08	0.00	35	0.00	0.77
SP_FDE_11	0.00	45	0.00	1.1
SP_FDE_12	0.00	50	0.00	1.2
SP_TP4_00	4.0	0.00	0.00	0.00
SP_FDE_TP4_04	4.0	19	0.00	0.40
SP_FDE_TP4_06	4.0	28	0.00	0.60
SP_FDE_TP4_08	4.0	35	0.00	0.80
SP_FDE_TP4_10	4.0	42	0.00	1.0
SP_FDE_TP4_12	4.0	48	0.00	1.2
SP_FDE9_AE_10	0.00	38	4.2	1.0
SP_FDE4_AE_10	0.00	33	8.2	1.0
SP_FDE2_AE_10	0.00	26	13	1.0
SP_FDE4_AE_12	0.00	37	9.2	1.2
SP_FDE9_AE_TP4_10	4.1	36	4.0	1.0
SP_FDE4_AE_TP4_10	4.2	32	7.9	1.0
SP_FDE2_AE_TP4_10	4.1	25	12	1.0
SP_FDE4_AE_TP4_12	4.0	36	8.8	1.2
EP_00	0.00	0.00	0.00	0.00
EP_FDE_04	0.00	17	0.00	0.40
EP_FDE_06	0.00	24	0.00	0.60
EP_FDE_08	0.00	31	0.00	0.80
EP_FDE_10	0.00	38	0.00	1.0
EP_FDE_12	0.00	44	0.00	1.2
EP_TP4_00	3.8	0.00	0.00	0.00
EP_FDE_TP4_04	3.8	16	16	0.40
EP_FDE_TP4_06	3.8	23	23	0.60
EP_FDE_TP4_08	3.8	30	30	0.80
EP_FDE_TP4_10	3.8	36	0.00	1.0
EP_FDE_TP4_11	3.8	42	0.00	1.1
EP_FDE9_AE_10	0.00	34	3.8	1.0
EP_FDE4_AE_10	0.00	29	7.4	1.0
EP_FDE2_AE_10	0.00	23	12	1.0
EP_FDE4_AE_12	0.00	34	8.5	1.2
EP_FDE9_AE_TP4_10	2.6	33	3.7	1.0
EP_FDE4_AE_TP4_10	2.7	29	7.2	1.0
EP_FDE2_AE_TP4_10	3.0	22	11	1.0
EP_FDE4_AE_TP4_12	2.6	33	8.3	1.2

Table 33: An overview of the contact angles and roughness values used in the analysis of the effect of different roughness values on the WCA.

Sample	**WCA** [°]	**h** [μ**m**]	**h'**	**h"** [**Mm**$^{-1}$]
SP_00	86.0	0.115	0.0219	0.0249
SP_FDE_04	95.2	0.890	0.492	0.208
SP_FDE_06	98.5	0.485	1.09	3.57
SP_FDE_08	109	0.597	1.03	3.33
SP_FDE_11	120	0.459	0.936	3.29
SP_FDE_12	122	0.438	0.982	3.56
SP_TP4_00	96.3	0.169	0.159	0.112
SP_FDE_TP4_04	90.2	1.23	1.46	0.647
SP_FDE_TP4_06	108	0.544	1.60	4.84
SP_FDE_TP4_08	117	0.457	1.32	4.18
SP_FDE_TP4_10	117	0.590	1.28	4.36
SP_FDE_TP4_12	88.6	1.11	1.25	4.46
SP_FDE9_AE_10	108	0.361	1.17	3.94
SP_FDE4_AE_10	105	0.468	1.45	4.29
SP_FDE2_AE_10	103	0.657	1.11	2.40
SP_FDE4_AE_12	113	0.427	1.27	4.17
SP_FDE9_AE_TP4_10	115	1.09	1.26	4.26
SP_FDE4_AE_TP4_10	120	0.533	1.12	3.52
SP_FDE2_AE_TP4_10	120	0.865	0.873	2.13
SP_FDE4_AE_TP4_12	116	0.824	0.940	2.87
EP_00	64.9	0.170	0.0241	0.0237
EP_FDE_04	74.1	0.883	0.102	0.0430
EP_FDE_06	72.8	1.11	1.21	0.475
EP_FDE_08	88.1	0.476	1.17	2.83
EP_FDE_10	106	0.759	1.26	3.90
EP_FDE_12	114	1.14	1.34	4.44
EP_TP4_00	93.2	0.442	0.0913	0.0786
EP_FDE_TP4_04	86.5	0.477	0.360	0.531
EP_FDE_TP4_06	83.7	0.560	1.23	0.134
EP_FDE_TP4_08	110	0.583	1.55	4.02
EP_FDE_TP4_10	118	0.802	1.59	5.26
EP_FDE_TP4_11	124	2.57	1.61	5.63
EP_FDE9_AE_10	74.8	0.376	1.35	4.13
EP_FDE4_AE_10	73.5	0.169	1.30	3.84
EP_FDE2_AE_10	78.4	0.529	1.19	2.33
EP_FDE4_AE_12	70.6	0.780	1.49	4.87
EP_FDE9_AE_TP4_10	108	0.600	1.30	3.69
EP_FDE4_AE_TP4_10	87.5	0.520	1.35	3.16
EP_FDE2_AE_TP4_10	90.6	0.508	1.33	2.57
EP_FDE4_AE_TP4_12	104	0.609	1.35	4.28

B Script for calculating master PSDF, h, h' and h"

```
import matplotlib.pyplot as plt
import numpy as np
import pandas as pd
from scipy.interpolate import interp1d
import scipy.integrate as integrate
from scipy import signal

#Function to calculate new spatial frequencies so the different PSDs have the same spatial frequencies
def newkfunc(k, oldk):
    newk = []
    for i in k:
        if i < oldk[-1]:
            newk.append(i)
        else:
            break
    return newk


def masterPSD(textfile):
    #Retrieve data
    data = np.array(pd.read_csv(textfile, delim_whitespace=True)) #usecols=[2,3,4,5,6,7] to ignore 1000nm

    #Create a function C(q) of the PSDFs
    fW = []
    for i in range(int(len(data[0,:])/2)):
        fW.append(interp1d(data[:,i*2], data[:,i*2+1]))


    #Create new spatial frequency values
    limit = data[-1,-2]
    n = int(limit/data[1,0])
    kmax = np.linspace(0, limit, n)
    k = []
    for i in range(int(len(data[0,:])/2)):
        k.append(newkfunc(kmax, data[:,i*2]))
    k.append(kmax)
    k = np.array(k)

    #Calculate new values for the intensity for the new spatial frequencies
    W = []
    for i in range(int(len(data[0,:])/2)):
        fWi = fW[i]
        W.append(fWi(k[i]))

    #Hann windowing to account for low accuracy for high and low spatial frequencies
    w = []
    for i in range(int(len(data[0,:])/2)):
        w.append(signal.get_window('hann', len(k[i])))

    #Changing list to array
    W = np.array(W)
    w = np.array(w)

    masterPSD = [W[0][0]]

    #Calculating the masterPSD by geometric weighing.
    for i in range(int(len(data[0,:])/2)): #Loop through n times for combining n PSDFs
```

```
58          if i == 0: #Special case for the very first loop
59              for j in range(len(k[i])):
60                  wPSD = 1
61                  wtot = 0
62                  for l in range(int(len(data[0,:])/2)):
63                      wtot += w[l][j]
64                      if wtot != 0:
65                          wPSD *= W[l][j]**w[l][j]
66                  if wtot != 0:
67                      wPSD = wPSD**(1/wtot)
68                      masterPSD.append(wPSD)
69              continue
70          if i == (int(len(data[0,:])/2)-1): #Special case for the very last
    loop
71              for j in range(len(k[i-1]), len(k[i])):
72                  masterPSD.append(W[i][j]*w[i][j])
73              break
74          if len(k[i]) == len(k[i-1]): #Special case if the ith PSD is of the
     same length as the (i-1)th PSD
75              print(i)
76              continue
77          for j in range(len(k[i-1]), len(k[i])): #This is the way one
    calculates the masterPSD when there is no special case
78              wPSD = 1
79              wtot = 0
80              for l in range(int(len(data[0,:])/2)-1, i-1, -1,): #Loop
    backwards from the ith to the 0th PSD
81                  wtot += w[l][j]
82                  wPSD *= W[l][j]**w[l][j]
83              wPSD = wPSD**(1/wtot)
84              masterPSD.append(wPSD)
85
86      masterPSD.append(masterPSD[-1])
87      masterPSD = np.array(masterPSD)
88
89
90      #Plot individudal and master PSDF
91      for i in range(int(len(data[0,:])/2)):
92          plt.plot(data[:,i*2],data[:,i*2+1])
93      plt.plot(k[-1], np.array(masterPSD))
94      plt.xlabel("Spacial frequency, q [m$^{-1}$]")
95      plt.ylabel("PSD (C$^{1D+}$) [m$^3$]")
96      plt.legend(["PSD 1000nm","PSD 250nm","PSD 100nm","PSD 25nm","Master PSD
    "])
97      plt.loglog()
98      plt.savefig(textfile+".pdf", dpi=250)
99      plt.show()
100
101
102     return masterPSD, k[-1]
103
104
105
106 mPSD, k = masterPSD("result2\ASE29\ASE29_PSDF")
107
108 #Calculating values for h, h' and h''
109 int_height = interp1d(k, mPSD)
110 int_slope = interp1d(k, mPSD*(k**2))
111 int_curvature = interp1d(k, mPSD*(k**4))
112
113 Iheight = integrate.quad(int_height, 0, 4500)
114 Islope = integrate.quad(int_slope, 0, k[-1])
115 Icurvature = integrate.quad(int_curvature, 0, k[-1])
```

```
116
117 height = np.sqrt(1/2*Iheight[0])
118 slope = np.sqrt(1/2*Islope[0])
119 curvature = np.sqrt(1/8*Icurvature[0])
```

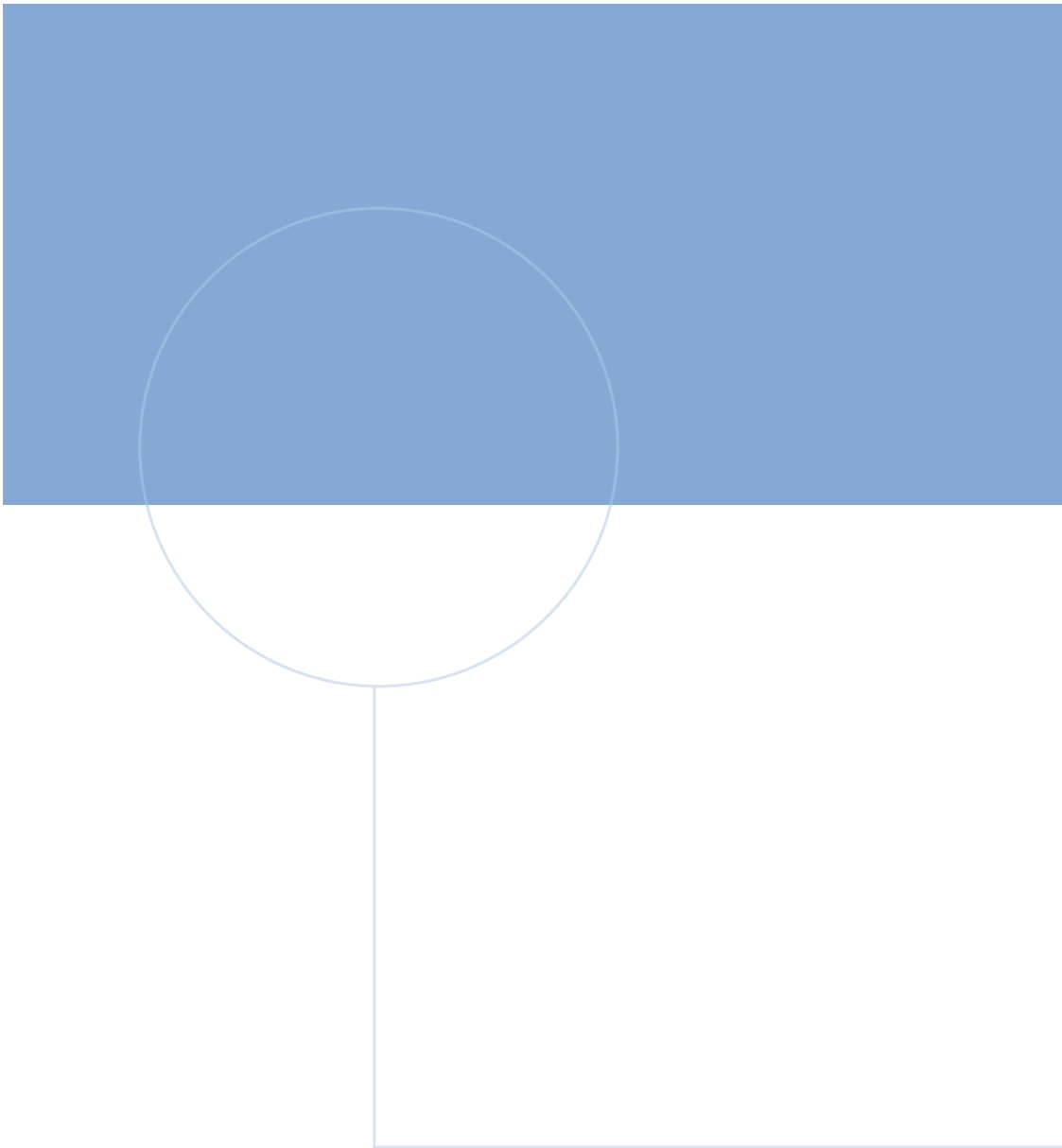

NTNU

Kunnskap for en bedre verden